SunShot
U.S. Department of Energy

CSP Program Summit 2016

An Integrated Coupled-Physics Framework for Performance and Life Prediction of Supercritical CO2 Turbomachines

energy.gov/sunshot

Azam Thatte, Lead Research Scientist - GE Global Research

Acknowledgements

* Work performed under U.S. DOE (EERE) PREDICTS program award # DE-EE0006345 .

Co-authors:
Adrian Loghin, Etienne Martin, Voramon Dheeradhada, Youngwon Shin, Balajee Ananthasayanam

Partners :
Southwest Research Institute (Jeff Moore, Tim Allison)

Overview

- FOA: PREDICTS (Physics of Reliability: Evaluating Design Insights for Component Technologies in Solar)
- Award Number:DE-EE0006345
- PI : Azam Thatte (GE Global Research)
- Partner : Southwest Research Institute
- Project Duration: Oct 2013 – Sept 2016
- Project Budget : $ 2.41 Million (20 % cost share by GE)

Problem Statement and Value Proposition

- Scalable Supercritical CO2 (sCO2) turbine expected to provide a major stepping stone for achieving CSP power at $0.06/kW-hr LCOE.
- Energy conversion efficiency > 50%, Total power block cost < $1,200/kW installed.
- Turbomachinery must have a 30-year life → ~ 11,000 thermal cycles.
- Under another Sunshot program (# DEEE0005804) GE and SWRI developing this 10MWe sCO2 turbine.
- Two key components critical to high efficiency of these sCO2 power cycles are:

1. Hybrid gas bearing (HGB).
2. Dry gas seal (DGS).

HGB→ ~ 5 % efficiency gain (rotordynamics & aero efficiency) , avoids 500 KW parasitic losses.

HGB → Allows integral compressor→ reduces cost.

DGS→ ~ 10 % improvement in efficiency (reduced leakage + generator windage)

DGS→ No need of multi-stage intercooled compressor to recompress leakage.

10 MWe GE-SWRI Sunshot sCO2 Turbine

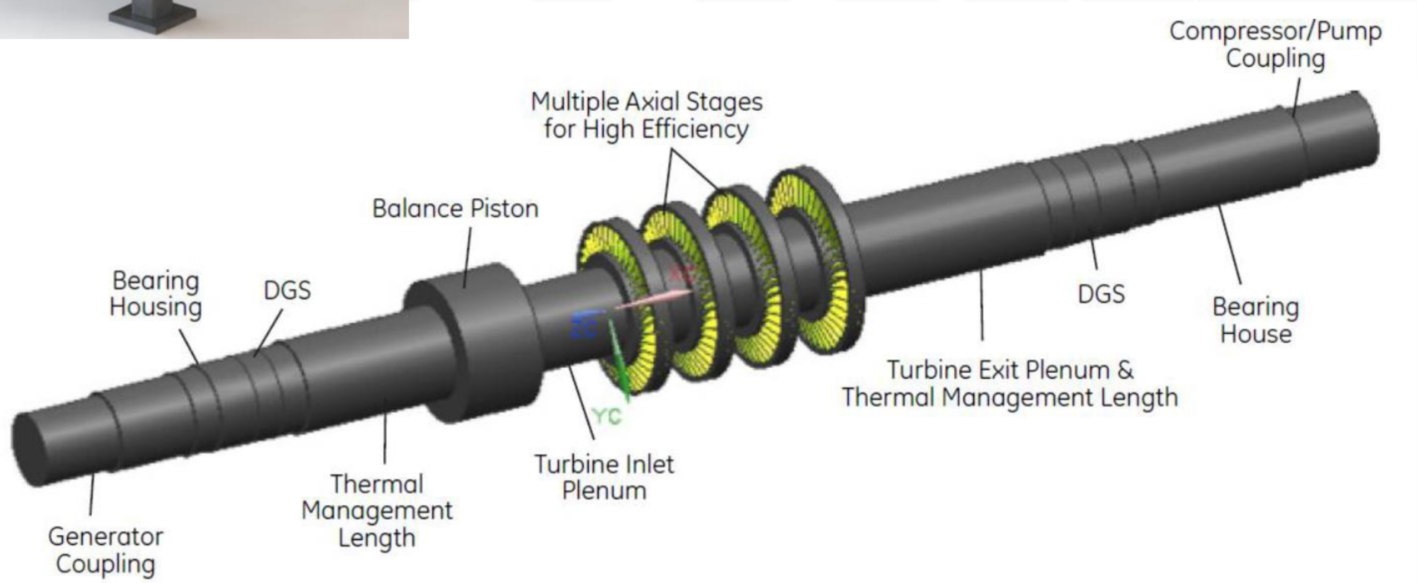

Why Hybrid Gas Bearing and Dry Gas Seal in sCO2 Turbines ?

- **Hybrid Gas Bearing** → ~ 3% efficiency gain
- Rotordynamics → Needs mid-span support for high power densities.
- Oil bearings need two sets of seals → combined parasitic load ~ 500 KW
- Larger L/D→ longer blades for same annular area→ aero efficiency
- No need of separate compressor package → reduced cost.

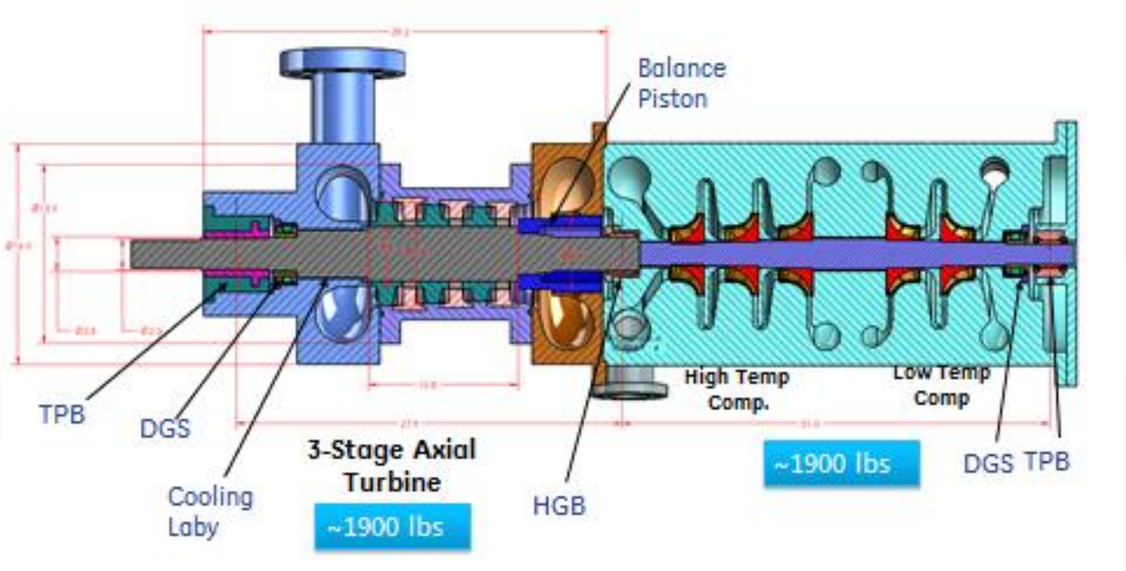

Why Hybrid Gas Bearing for sCO2 Turbine ?

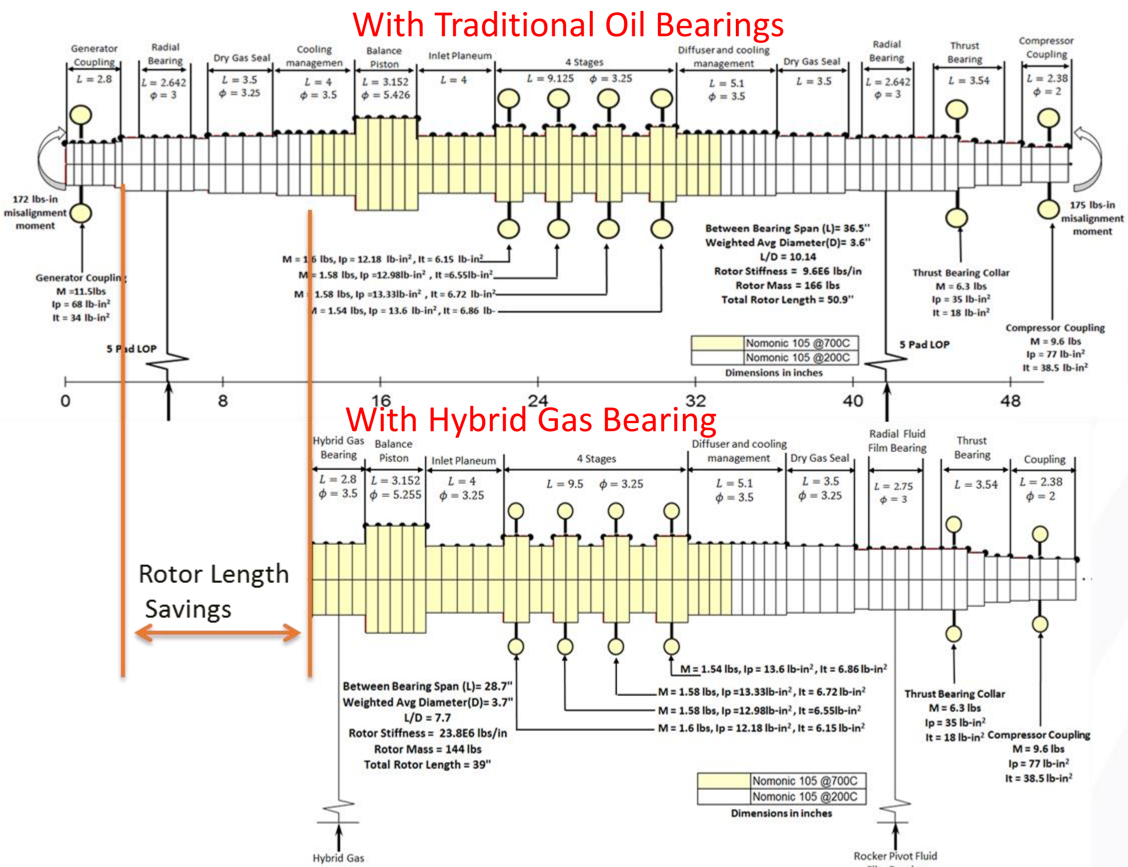

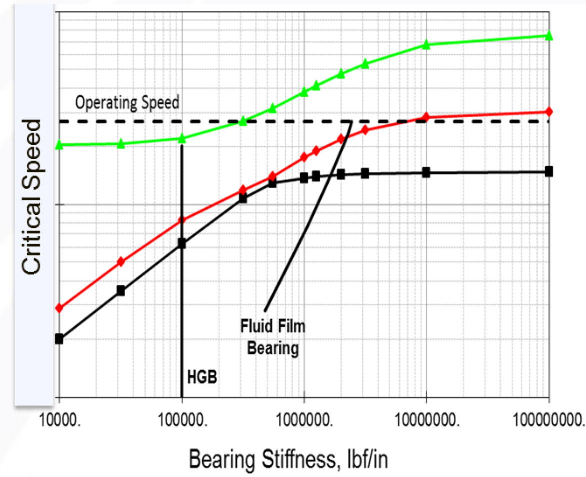

HGB brings sCO2 rotor down into comfortable CSR regime

$$CSR = \frac{continuous\ speed}{first\ UCS\ on\ rigid\ support\ (FCSR)}$$

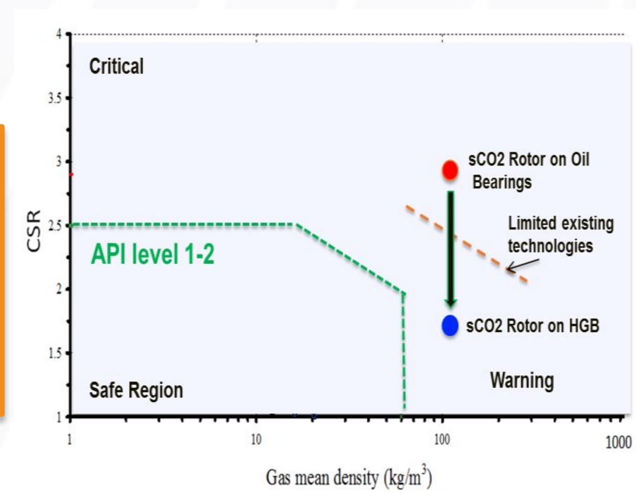

1) Shorter Rotor→ Reduced rotor flexibility→ rotordynamically stable
2) For same L/D, longer blades → aero efficiency.
3) No parasitic losses from seals → 500 KW
4) Gas less viscous→Lower power loss in the bearing
5) Midspan bearing allows integral compressor → reduced cost.

Why Dry Gas Seal in sCO2 Turbine ?

- ~ 10 % improvement in overall system efficiency (leakage + generator windage)

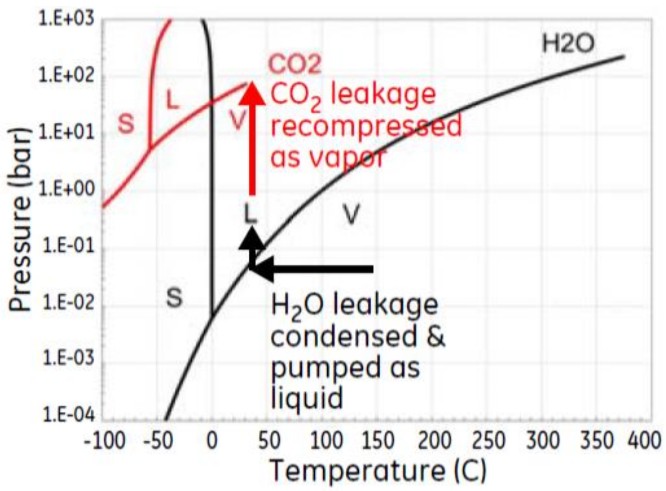

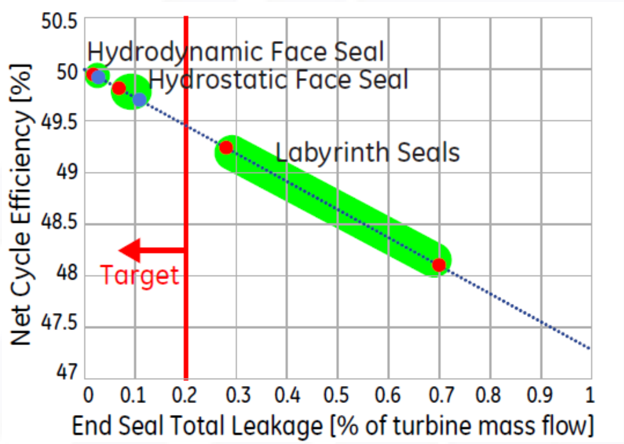

- Unlike steam Rankine cycles, leaked CO2 must be compressed as vapor back to main compressor inlet pressure of ~80 bar.

- Need multi-stage intercooled compressors → Large auxiliary compression load→ efficiency penalty (figure on right)

- 0.6% total end seal leakage reduces net cycle efficiency from 50% to about 48.4%.

- High temperature DGS→ eliminate need for thermal management schemes → reduce rotor span→ better L/D → better Aero efficiency & rotordynamics.

- Aid 500 MW scale sCO2 turbine designs by allowing 24-36" diameter DGS design which does not exists today.

Project Objectives

- Develop coupled physics performance and life prediction framework for sCO2 turbomachines

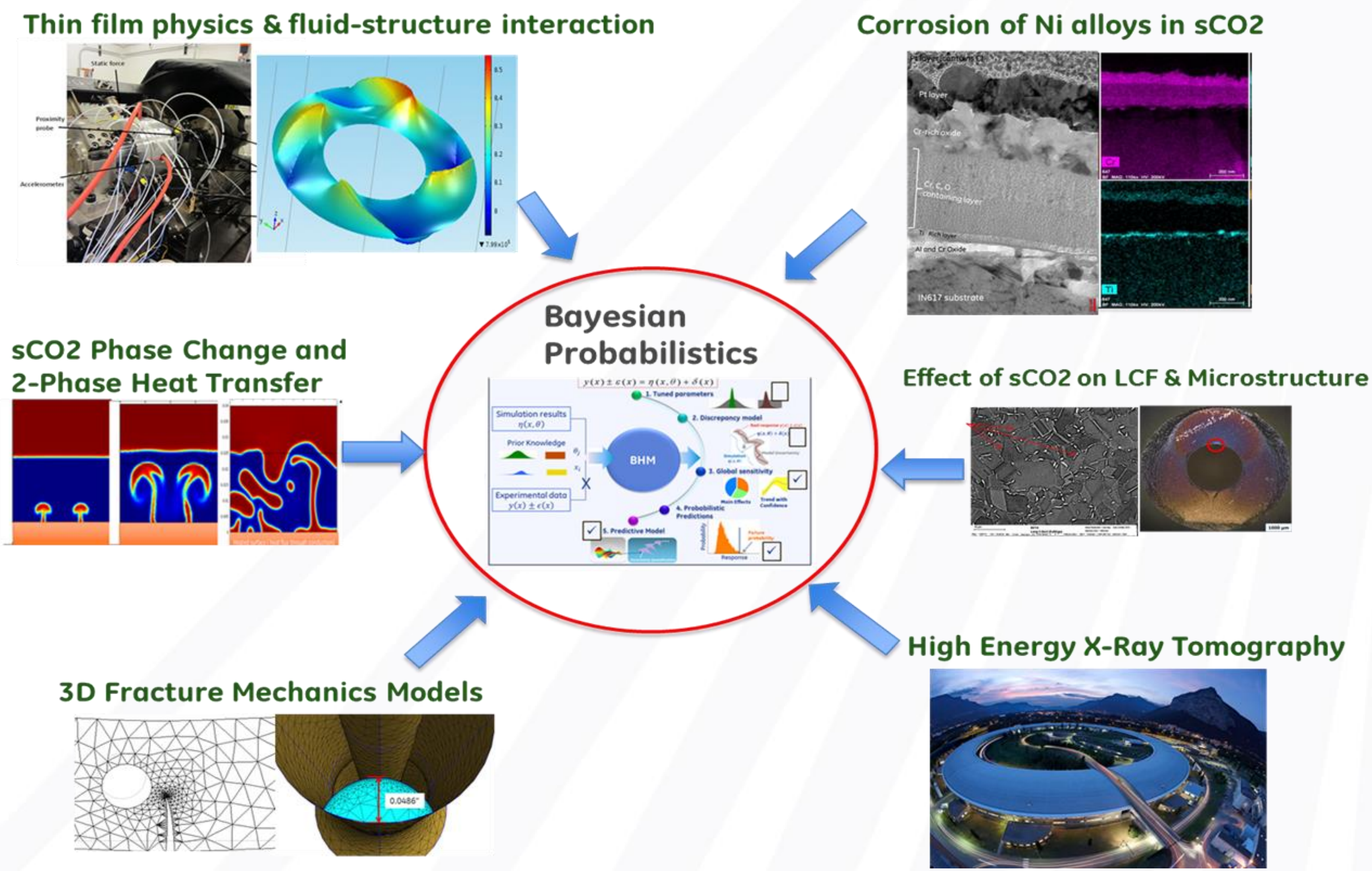

Hybrid Gas Bearing

- Combine hydrostatic and hydrodynamic load support
- Flexure pivot tilting pad bearing for stability
- Maintain very tight film thickness ~ mil
- Bearing is soft-mounted on s-Spring to provide compliance.
- Damping is achieved between the pad and supports via wire mesh to dissipate vibration energy

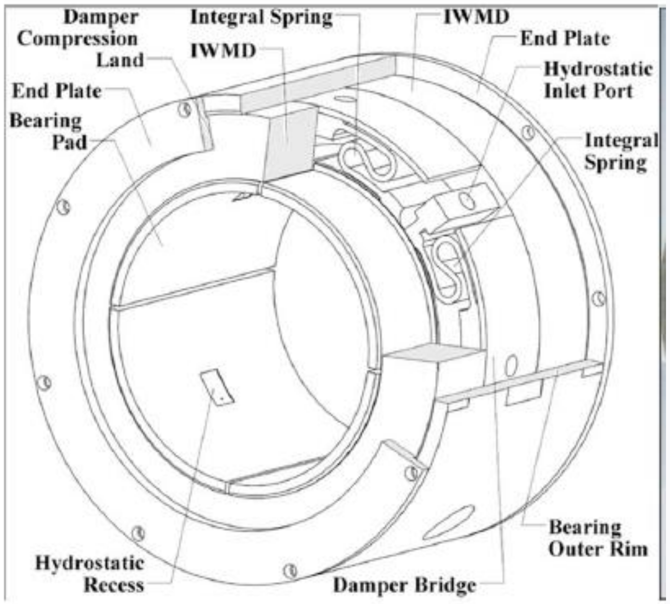

Hybrid Gas Bearing Performance Model

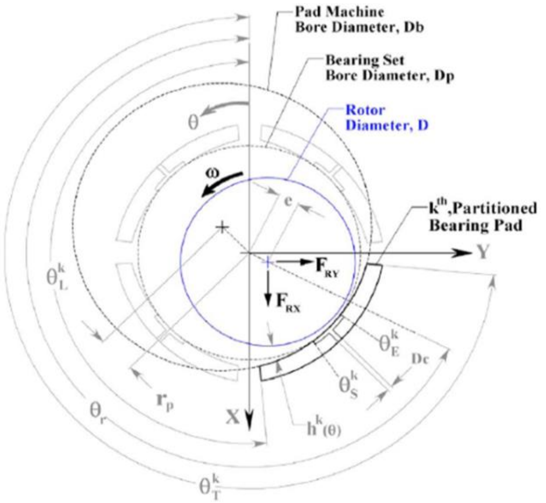

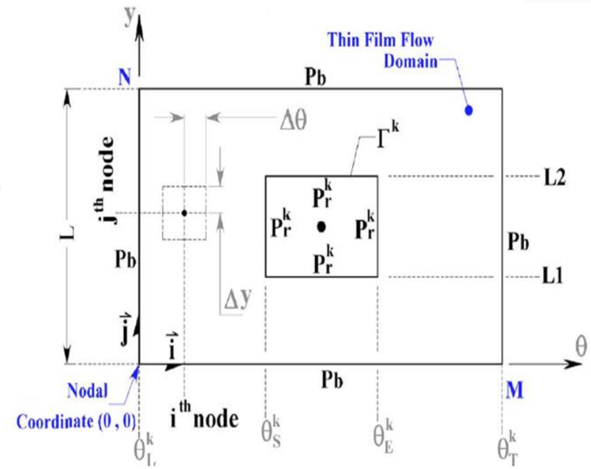

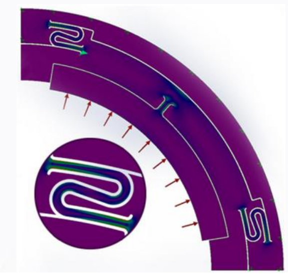

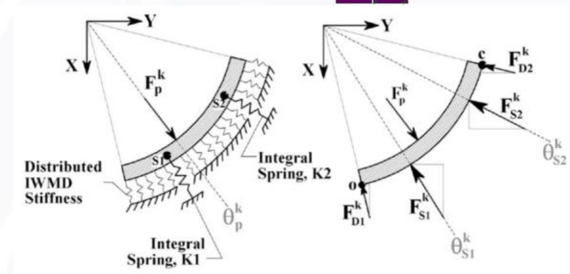

- Static Pressure: flow from supply pressure tube to bearing edge (guess recess pressure) .
- Guess rotor position → determine film thickness → solve compressible Reynolds equation .
- Wire mesh damping and stiffness properties determined experimentally.
- Structural stiffness and damping matrices constructed from X,Y force equilibrium

$$\begin{bmatrix} F^k_{PX} \\ F^k_{PY} \end{bmatrix} = \int_0^L \int_{\theta^k_L}^{\theta^k_T} (P^k - P_b) \begin{bmatrix} \cos\theta \\ \sin\theta \end{bmatrix} \cdot R d\theta \cdot dy$$

$$F^k_p \cdot \begin{bmatrix} \sin\theta^k_p \\ \cos\theta^k_p \end{bmatrix} = F^k_{D1} \cdot \begin{bmatrix} \sin\theta^k_L \\ \cos\theta^k_L \end{bmatrix} + F^k_{D2} \cdot \begin{bmatrix} \sin\theta^k_T \\ \cos\theta^k_T \end{bmatrix} + F^k_{S1} \cdot \begin{bmatrix} \sin\theta^k_{S1} \\ \cos\theta^k_{S1} \end{bmatrix} + F^k_{S2} \cdot \begin{bmatrix} \sin\theta^k_{S2} \\ \cos\theta^k_{S2} \end{bmatrix}$$

$$\dot{m}^k_C = C_D \cdot \frac{\left(\frac{D_C}{2}\right)^2 \cdot \pi \cdot P_s}{\sqrt{\gamma \cdot \Re \cdot T}} \cdot \sqrt{\frac{2 \cdot \gamma^2}{\gamma - 1} \cdot \left[\left(\frac{P^k_r}{P_s}\right)^{2/\gamma} - \left(\frac{P^k_r}{P_s}\right)^{(\gamma+1)/\gamma} \right]}$$

$$\dot{m}_{\text{choked}} = \left(\frac{2}{\gamma+1}\right)^{1/(\gamma-1)} \cdot \sqrt{\frac{\gamma-1}{\gamma+1}} \cdot \frac{\left(\frac{D_C}{2}\right)^2 \cdot \pi \cdot P_s}{\sqrt{\gamma \cdot \Re \cdot T}} \sqrt{\frac{2 \cdot \gamma^2}{\gamma - 1}}$$

$$h^k = C + e_X \cos(\theta) + e_Y \sin(\theta) - r_P \cos\left(\theta - \frac{(\theta^k_T - \theta^k_L)}{2}\right)$$

$$\frac{1}{R^2}\frac{\partial}{\partial\theta}\left((h^k)^3 P^k \frac{\partial P^k}{\partial\theta}\right) + \frac{\partial}{\partial y}\left((h^k)^3 P^k \frac{\partial P^k}{\partial y}\right) = 6\mu\omega\frac{\partial}{\partial\theta}(h^k P^k)$$

Hybrid Gas Bearing Performance in sCO2 Turbine

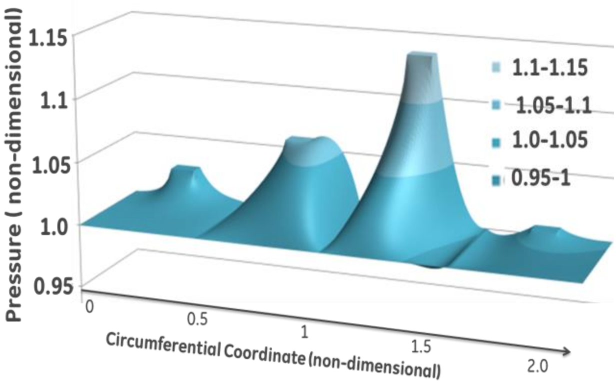

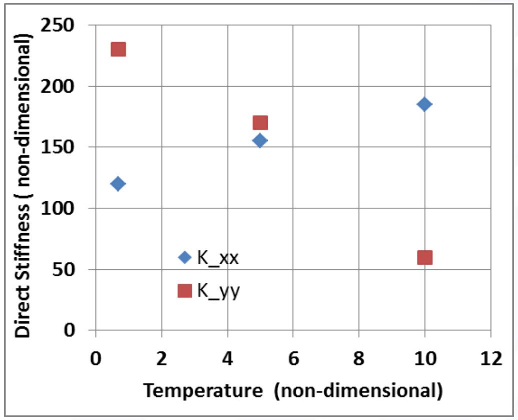

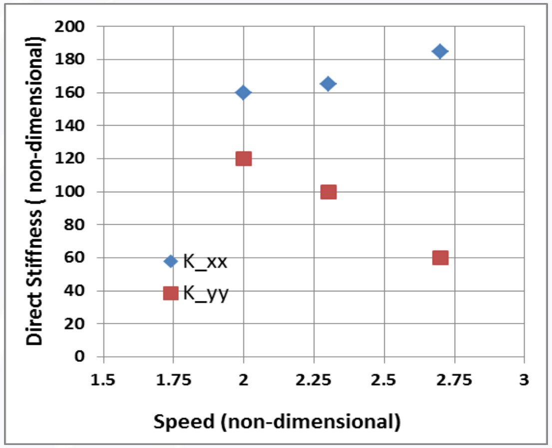

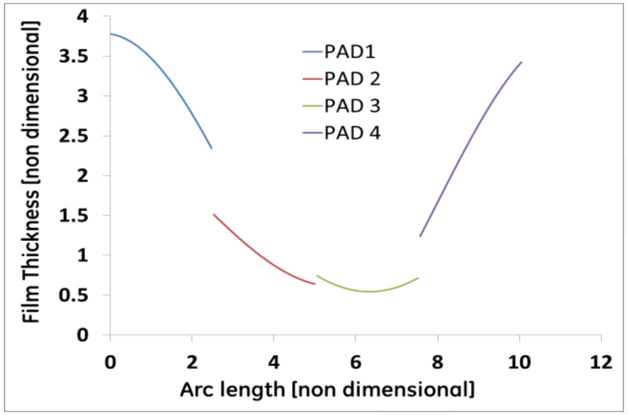

Non-dimensional stiffness of HGB during sCO2 operation	Non-dimensional damping of HGB during sCO2 operation
Kxx = 235	Cxx = 89
Kxy = -2.6	Cxy = 21
Kyx = -5.1	Cyx = 29
Kyy= 312	Cyy= 48

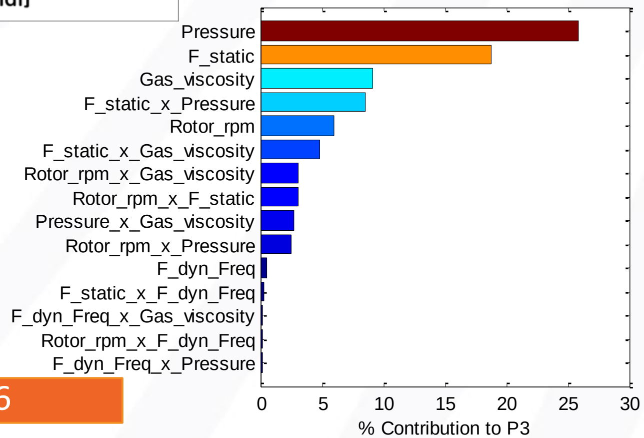

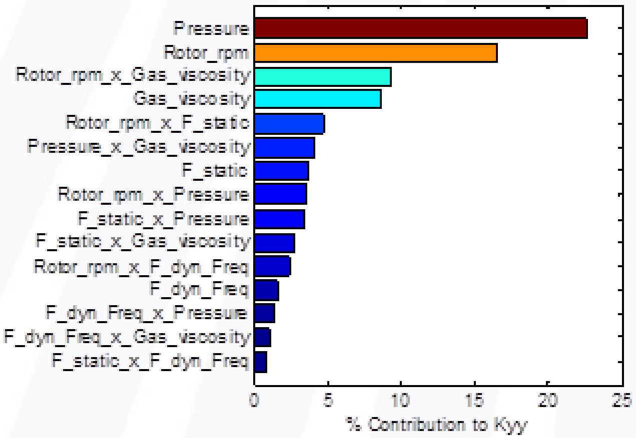

Model Validation (in Air) using Pressurized Rotordynamics Tests on Hybrid Gas Bearing

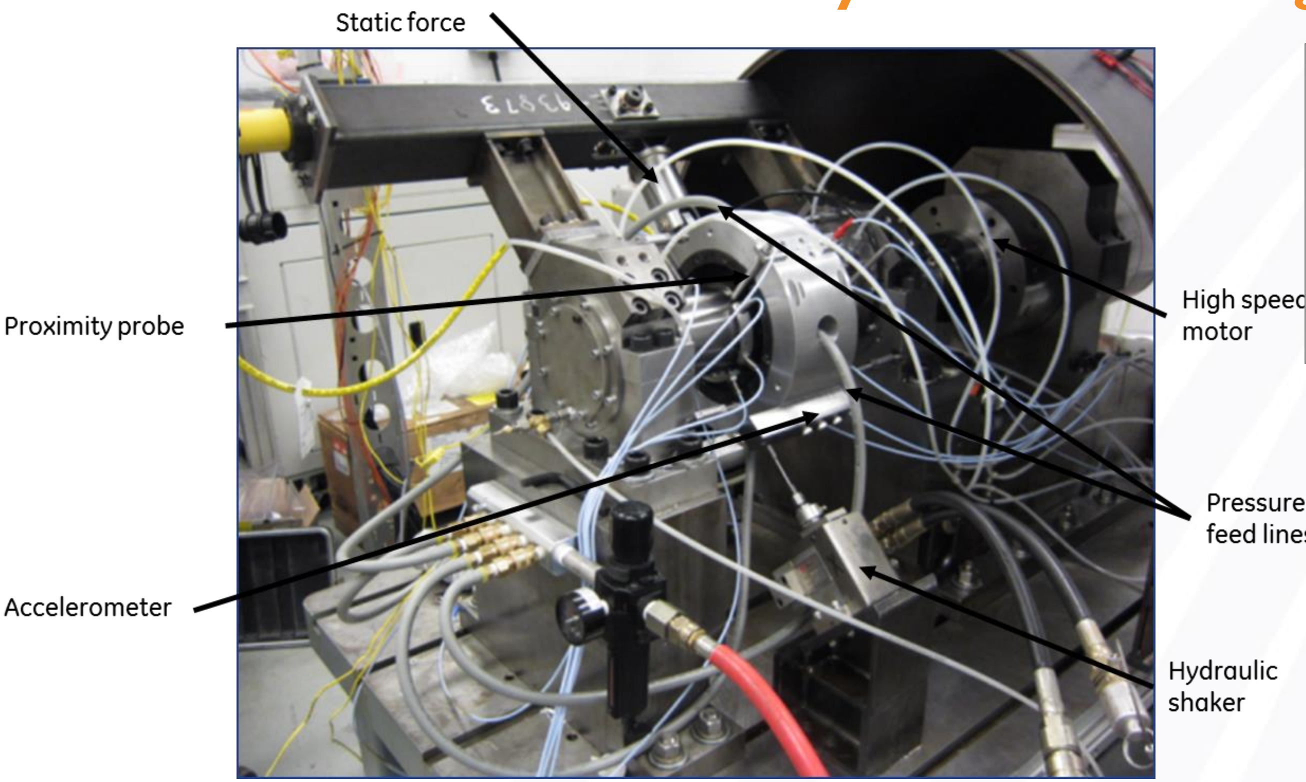

Pad rotations

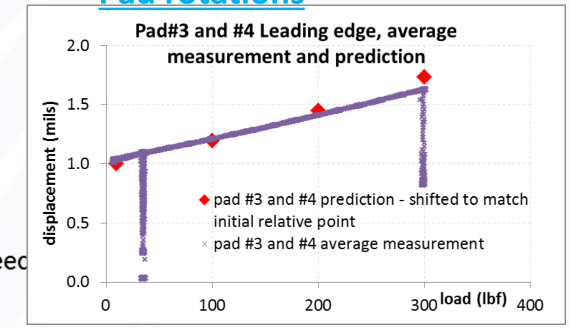

High resolution strain gages

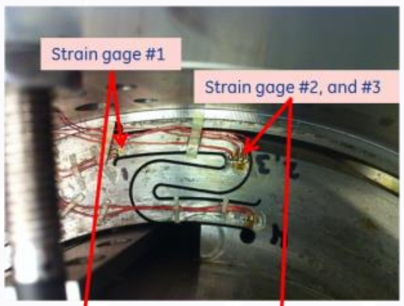

Strain in S-Springs

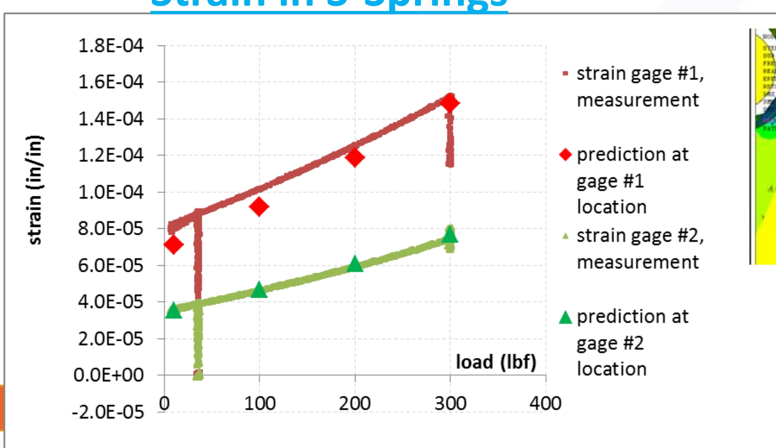

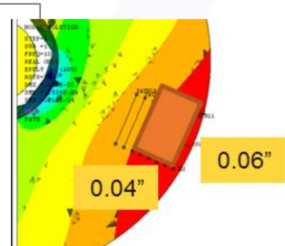

Large orbit single frequency excitations → Bearing response due to unbalance

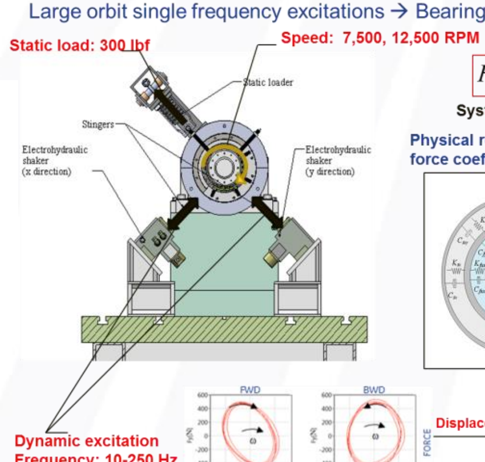

Parameter Identification

$$H_{ij}(\omega) = K_{ij} - \omega^2 M_{ij} + i\omega\left(C_{ij}\right)$$

System’s complex dynamic stiffness

Physical representation of rotor-bearing system’s force coefficients:

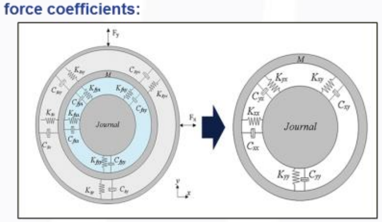

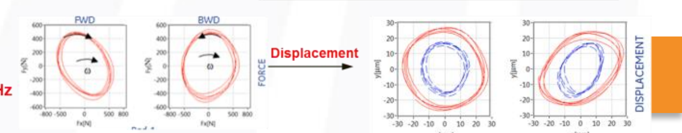

Hybrid Gas Bearing Load Mission in sCO2 Turbine

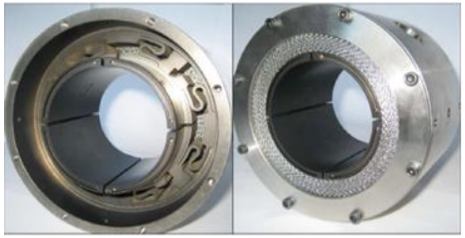

Coupled Fluid-Structure-Thermal Interactions in sCO2

$$\dot{m}_C^k = C_D \cdot \frac{\left(\frac{D_C}{2}\right)^2 \cdot \pi \cdot P_s}{\sqrt{\gamma \cdot \Re \cdot T}} \cdot \sqrt{\frac{2\cdot\gamma^2}{\gamma-1} \cdot \left[\left(\frac{P_r^k}{P_s}\right)^{2/\gamma} - \left(\frac{P_r^k}{P_s}\right)^{(\gamma+1)/\gamma}\right]}$$

$$\dot{m}_{\text{choked}} = \left(\frac{2}{\gamma+1}\right)^{1/(\gamma-1)} \cdot \sqrt{\frac{\gamma-1}{\gamma+1}} \cdot \frac{\left(\frac{D_C}{2}\right)^2 \cdot \pi \cdot P_s}{\sqrt{\gamma \cdot \Re \cdot T}} \sqrt{\frac{2\cdot\gamma^2}{\gamma-1}}$$

$$h^k = C + e_X \cos(\theta) + e_Y \sin(\theta) - r_P \cos\left(\theta - \frac{(\theta_T^k - \theta_L^k)}{2}\right)$$

$$\frac{1}{R^2}\frac{\partial}{\partial\theta}\left((h^k)^3 P^k \frac{\partial P^k}{\partial\theta}\right) + \frac{\partial}{\partial y}\left((h^k)^3 P^k \frac{\partial P^k}{\partial y}\right) = 6\mu\omega\frac{\partial}{\partial\theta}(h^k P^k)$$

$$\bar{y} = \frac{y}{D},\quad \bar{P}^k = \frac{P^k}{P_b},\quad \bar{h}^k = \frac{h^k}{C},\quad \Lambda = \frac{6\mu\omega}{P_b}\left(\frac{R}{C}\right)^2$$

$$\left(\frac{\partial\bar{P}}{\partial\theta}\right)_{i,j} \approx \frac{\bar{P}_{i+1,j} - \bar{P}_{i-1,j}}{\theta_{i+1} - \theta_{i-1}} = \frac{\bar{P}_{i+1,j} - \bar{P}_{i-1,j}}{2\Delta\theta}$$

$$\left(\frac{\partial\bar{P}}{\partial\bar{y}}\right)_{i,j} \approx \frac{\bar{P}_{i,j+1} - \bar{P}_{i,j-1}}{\bar{y}_{j+1} - \bar{y}_{j-1}} = \frac{\bar{P}_{i,j+1} - \bar{P}_{i,j-1}}{2\Delta\bar{y}}$$

$$\left(\frac{\partial^2\bar{P}}{\partial\theta^2}\right)_{i,j} \approx \frac{\left(\frac{\partial\bar{P}}{\partial\theta}\right)_{i+1,j} - \left(\frac{\partial\bar{P}}{\partial\theta}\right)_{i,j}}{\theta_{i+1} - \theta_i} = \frac{\bar{P}_{i+1,j} - 2\bar{P}_{i,j} + \bar{P}_{i-1,j}}{(\Delta\theta)^2}$$

$$\left(\frac{\partial^2\bar{P}}{\partial\bar{y}^2}\right)_{i,j} \approx \frac{\left(\frac{\partial\bar{P}}{\partial\bar{y}}\right)_{i,j+1} - \left(\frac{\partial\bar{P}}{\partial\bar{y}}\right)_{i,j}}{\bar{y}_{j+1} - \bar{y}_j} = \frac{\bar{P}_{i,j+1} - 2\bar{P}_{i,j} + \bar{P}_{i,j-1}}{(\Delta\bar{y})^2}$$

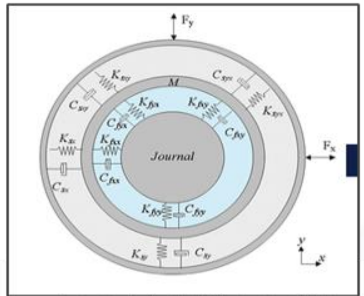

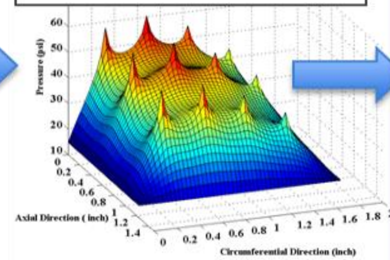

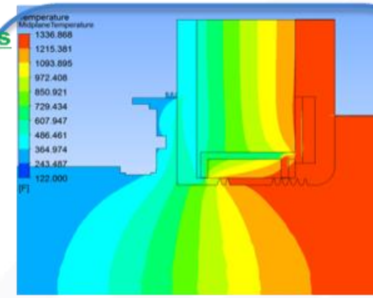

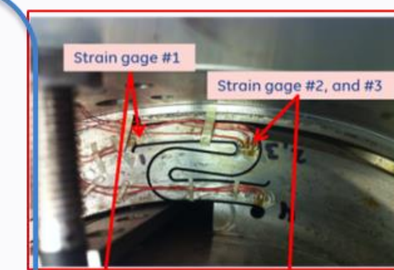

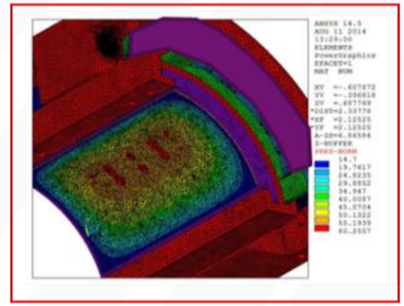

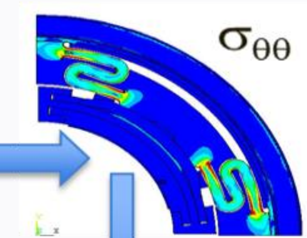

Turbine loading mission

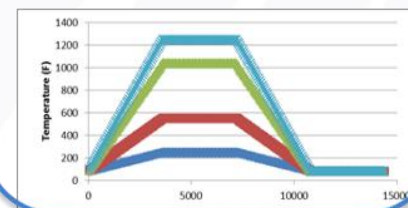

Validation Tests:

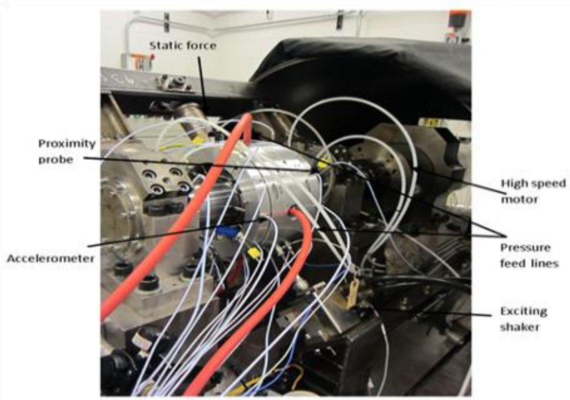

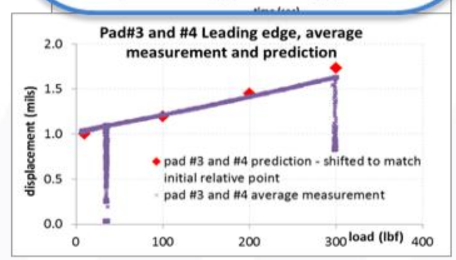

Total Life

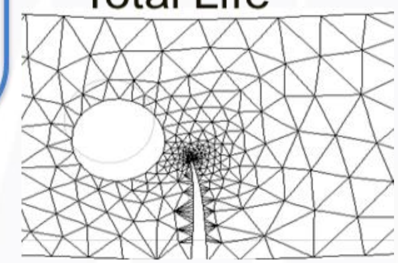

Thin Film Physics + Rotordynamics + System Level Fluid-Thermal-Structural → Loading Mission Cycle For Life Prediction

Dry Gas Seal Performance Models

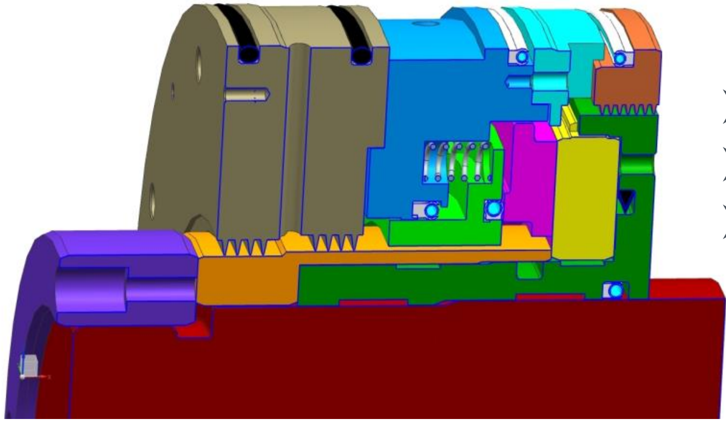

- Assess Performance Risks
- Feed into Life Model
- Design Optimization for large MW sCO2 turbines

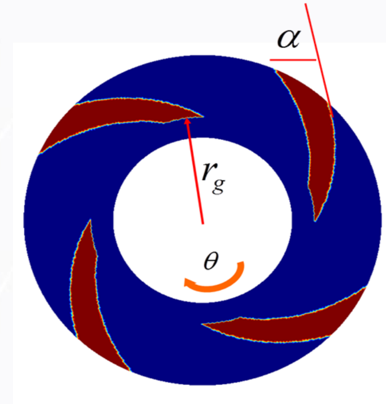

$$r = r_g e^{\theta \tan(\alpha)}$$

Thin Film Physics:

$$\frac{1}{r}\frac{\partial}{\partial\tilde{\theta}}\left(\frac{p\,h^3}{\mu}\frac{\partial P}{\partial\tilde{\theta}}\right)+\frac{\partial}{\partial r}\left(r\,\frac{p\,h^3}{\mu}\frac{\partial P}{\partial r}\right)=12\,\omega\,r\,\frac{\partial}{\partial\tilde{\theta}}(h\,p)$$

Coupled Fluid-Structure Interaction:

Seal (system) level

$$\boxed{\dot{\mathbf{x}}(t) = \underbrace{\begin{bmatrix}\mathbf{0}_{5N\times5N} & \mathbf{I}_{5N\times5N}\\ -\mathbf{M}^{-1}\mathbf{K} & -\mathbf{M}^{-1}\mathbf{C}\end{bmatrix}}_{10N\times10N}\mathbf{x}(t)+\mathbf{b}(\mathbf{x},t)} \qquad \mathbf{x} = \begin{pmatrix}\mathbf{y}\\ \dot{\mathbf{y}}\end{pmatrix}_{10N\times1}$$

Segment Level

$$\mathbf{M} = \begin{bmatrix}\mathbf{M}_{11} & 0 & 0 & 0\\ 0 & \mathbf{M}_{ii} & 0 & 0\\ 0 & 0 & . & 0\\ 0 & 0 & 0 & M_{NN}\end{bmatrix} \quad \mathbf{K} = \begin{bmatrix}K_{11} & K_{12} & 0 & K_{14}\\ K_{21} & K_{22} & K_{23} & 0\\ & & . & \\ K_{N1} & & K_{(N-1)N} & K_{NN}\end{bmatrix} \quad \mathbf{y} = \begin{pmatrix}\mathbf{y}_1\\ .\\ \mathbf{y}_N\end{pmatrix}$$

DOF Level

$$\mathbf{K}_{ii} = \begin{bmatrix}k_{xx} & & & & \\ & kyy & & & \\ & & kzz & & \\ & & & k_{sy} & 0\\ & & & 0 & k_{sy}\end{bmatrix} \quad \mathbf{K}_{ij} = \begin{bmatrix}ki_{xx} & ki_{xy} & ki_{xz} & ki_{x\gamma} & ki_{x\gamma}\\ ki_{yx} & ki_{yy} & ki_{yz} & ki_{y\gamma} & ki_{y\gamma}\\ ki_{zx} & ki_{zy} & ki_{zz} & ki_{z\gamma} & k_{z\gamma}\\ ki_{\gamma x} & ki_{\gamma y} & ki_{\gamma x} & ki_{sy} & ki_{\gamma z}\\ ki_{\gamma x} & ki_{\gamma y} & ki_{zx} & ki_{zy} & k_{sy}\end{bmatrix}$$

$$\mathbf{M}_{ii} = \begin{bmatrix}m & 0 & 0 & 0 & 0\\ 0 & m & 0 & 0 & 0\\ 0 & 0 & m & 0 & 0\\ 0 & 0 & 0 & I_{xx} & I_{xy}\\ 0 & 0 & 0 & & \end{bmatrix} \qquad \mathbf{y}_i = \begin{pmatrix}x\\ y\\ z\\ \gamma_X\\ \gamma_Y\end{pmatrix}$$

Hydrodynamic Pressure at Interface

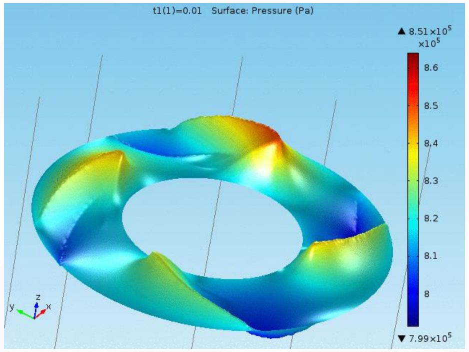

Effect of Turbine Axial Transients

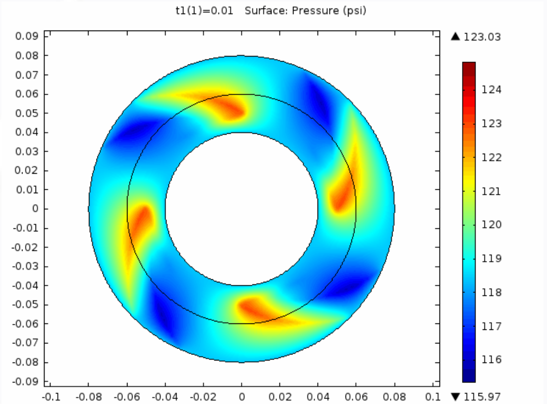

Tilt & Coning

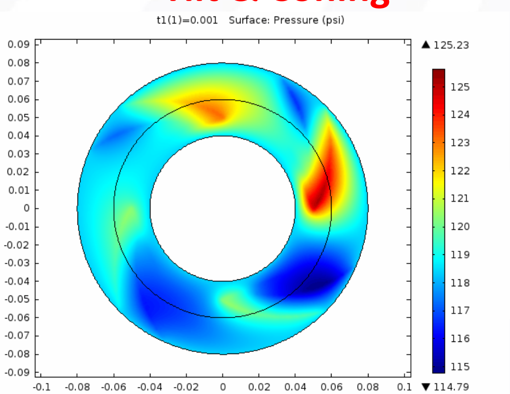

ND1 vibrations

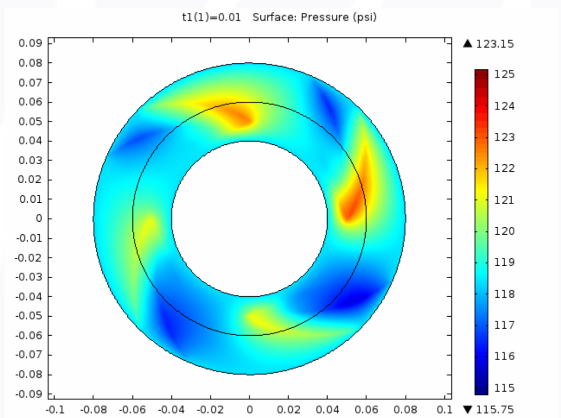

Hydrodynamic Force & Stiffness Variation with Spiral Angle

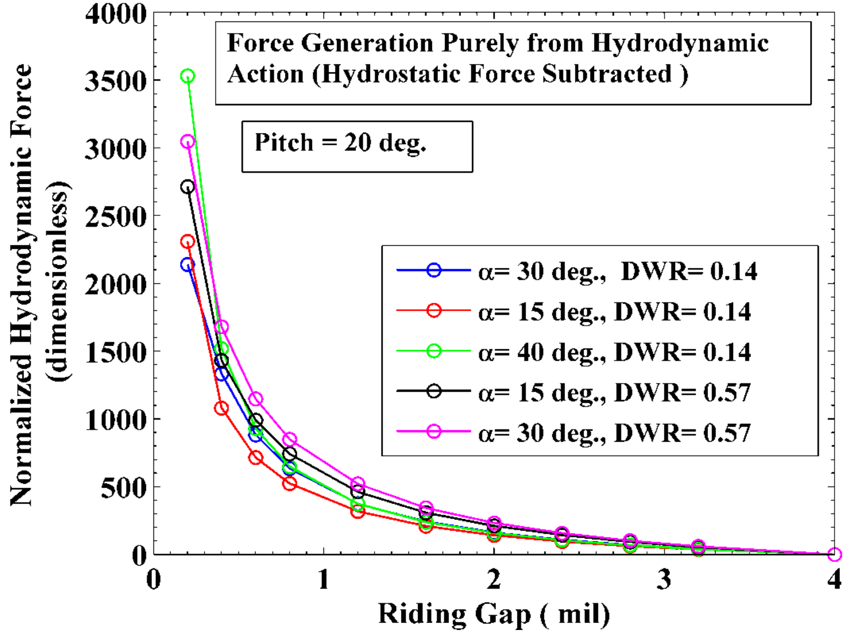

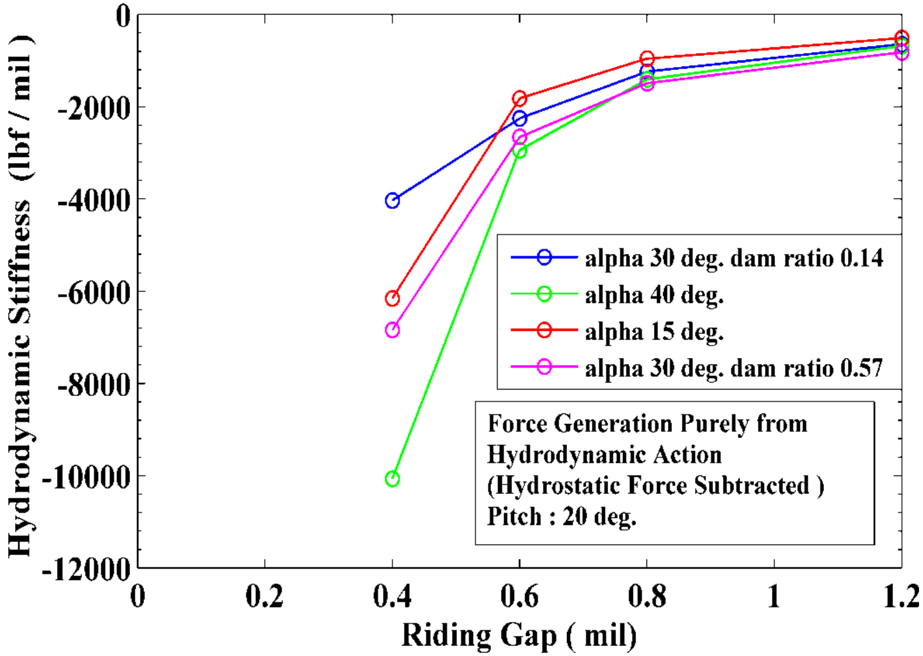

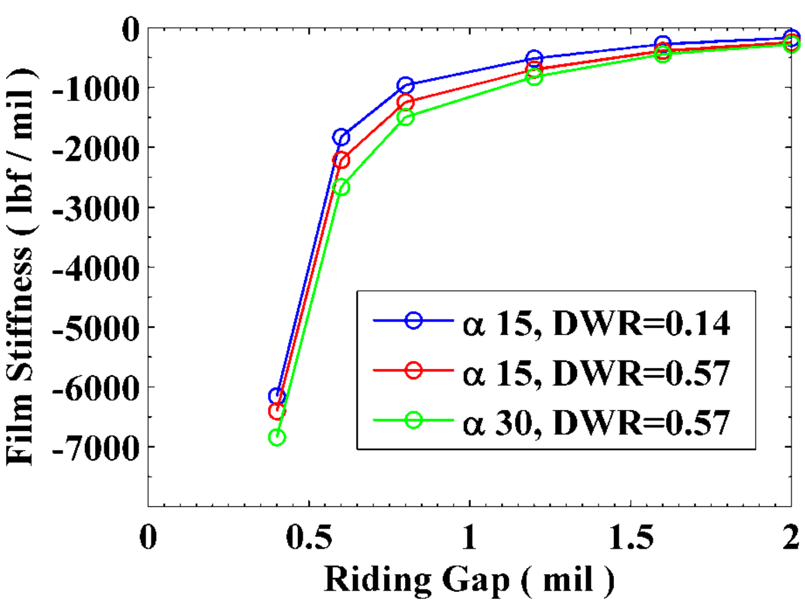

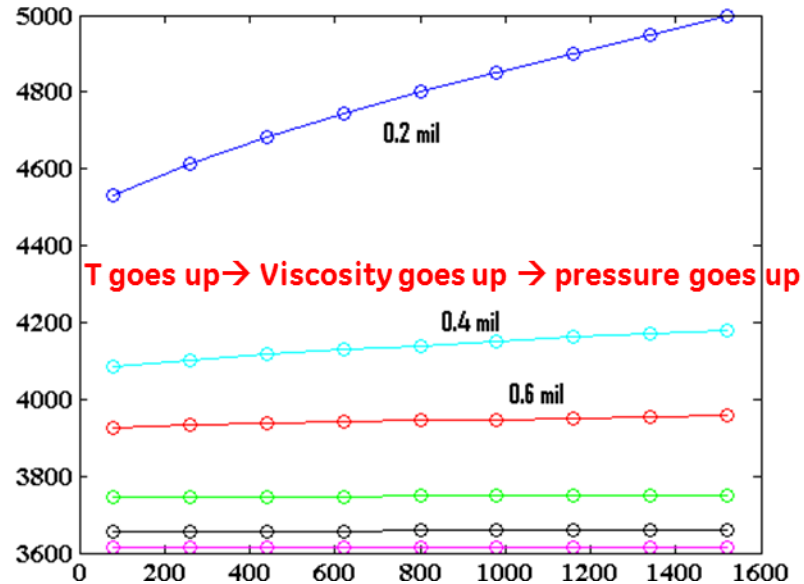

sCO2 Specific Perturbations

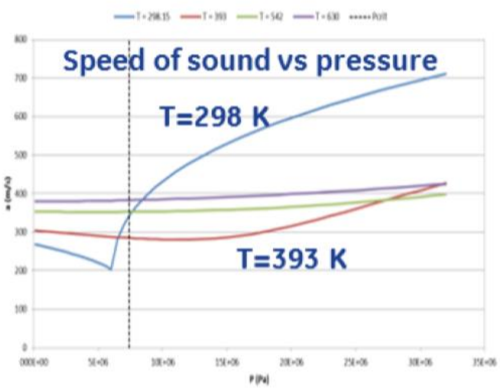

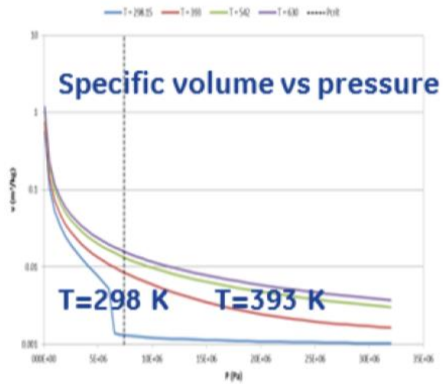

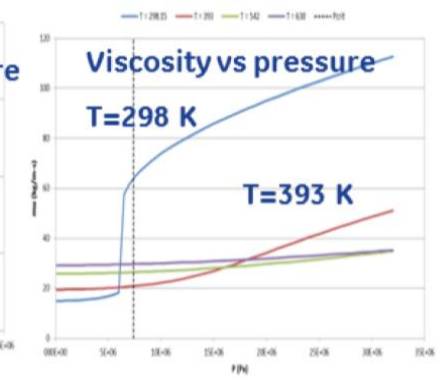

Sonic Transition

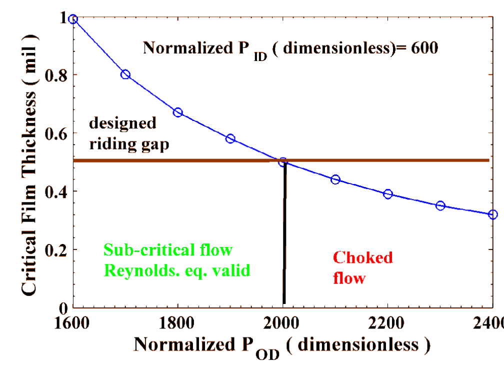

Density

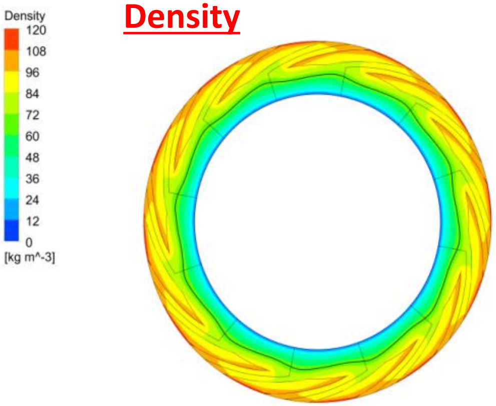

Speed of Sound

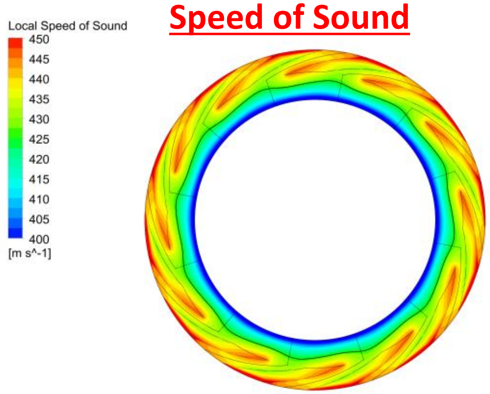

Risks addressed through Advanced Models

- Supercritical→ Liquid→ Dry Ice.
- Sonic Transition @ DGS interface
- Density→ Local speed of sound →Mach #
- High Biot # , High Nusselt # → Large thermal stresses, coning

Mach # Variation

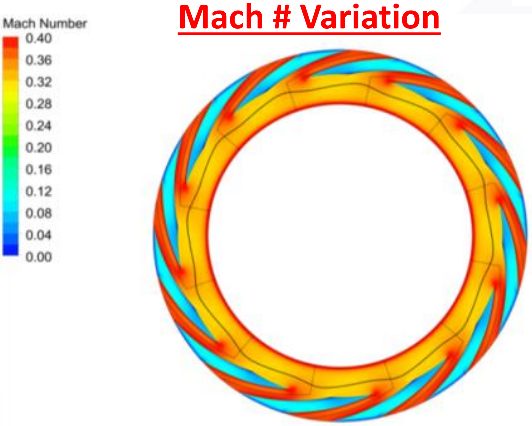

Thermal-Structural Risks

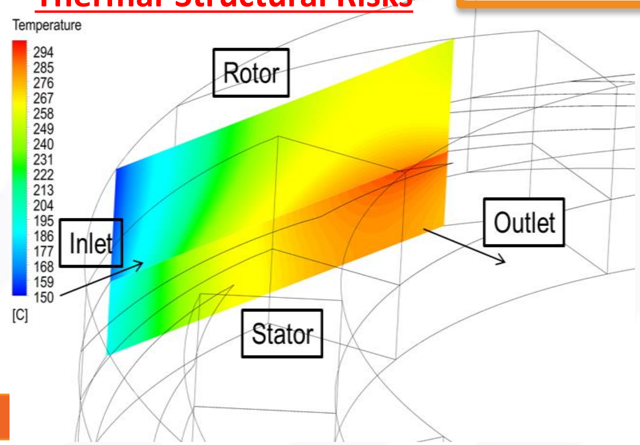

Flow Reversal

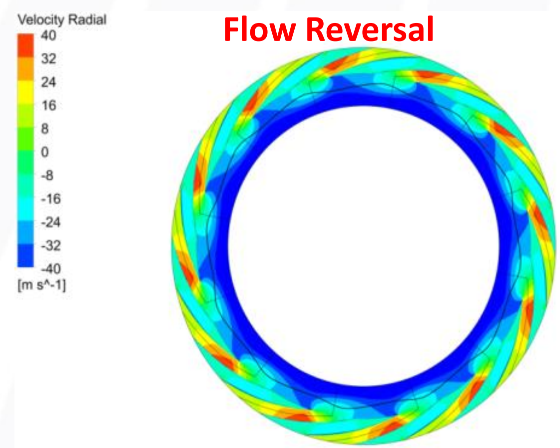

sCO2 Phase Change & Surface Tension Studies

sCO2 Phase Diagram

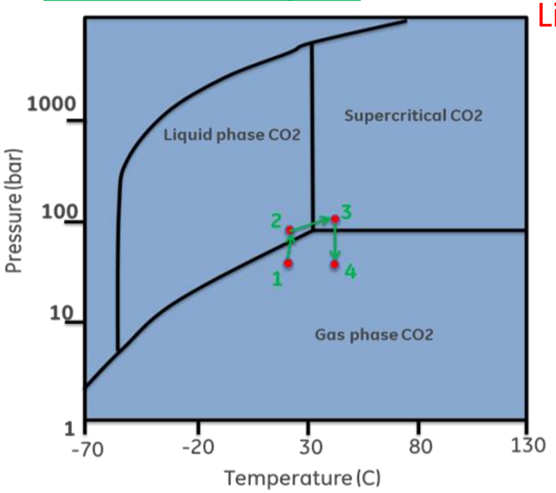

Pressurization Path (1→2→3)

Liquid-gas interface

No meniscus
→ No surface tension
→ Supercritical State

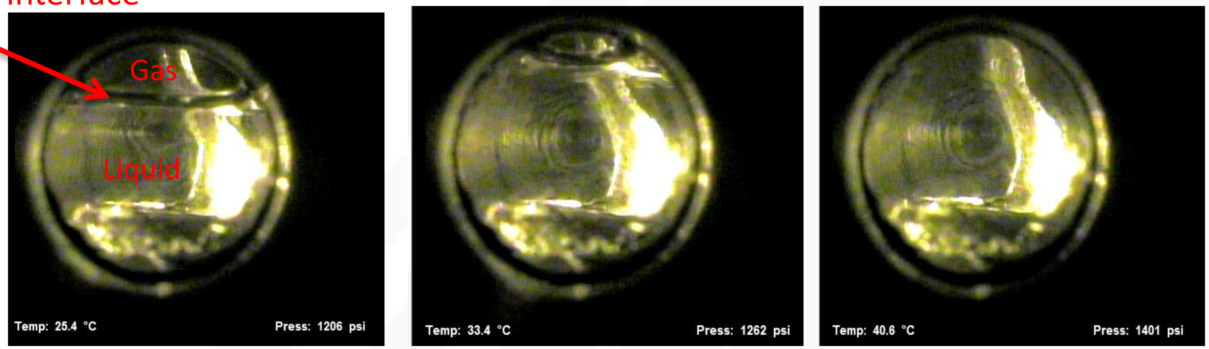

Experimental Setup

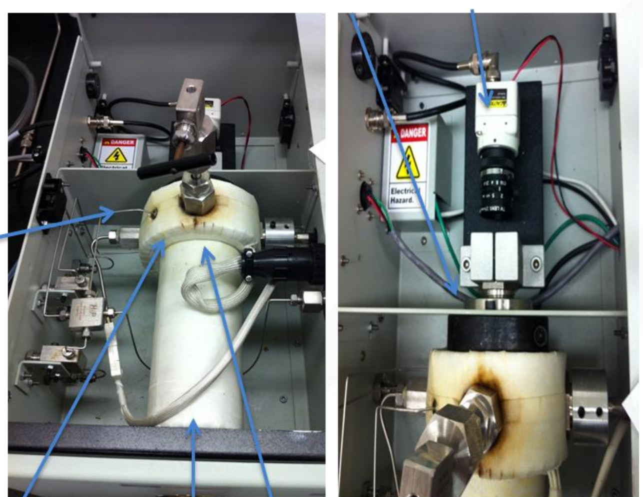

CO2 line

Pressure vessel

Heating circuit

Positive displacement pump

De-Pressurization Path (3→4)

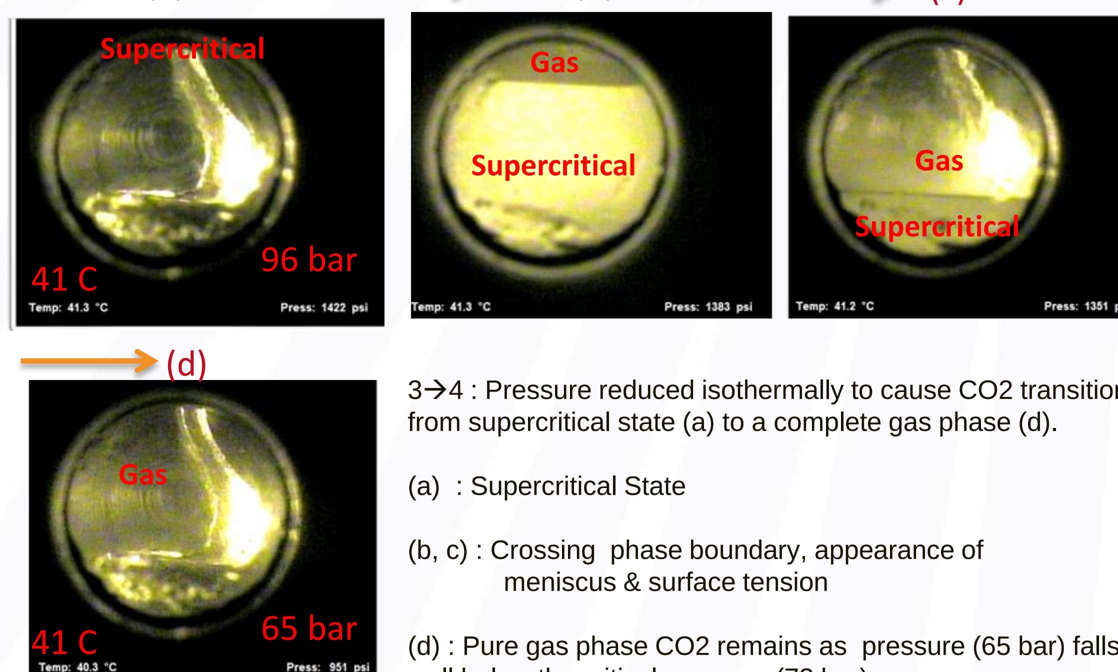

3→4 : Pressure reduced isothermally to cause CO2 transition from supercritical state (a) to a complete gas phase (d).

(a) : Supercritical State

(b, c) : Crossing phase boundary, appearance of meniscus & surface tension

(d) : Pure gas phase CO2 remains as pressure (65 bar) falls well below the critical pressure (73 bar).

Phase Change and 2-Phase Flow Model

Liquid phase described using incompressible Navier-Stokes equations:

$$\rho_L \frac{\partial \mathbf{u}_L}{\partial t} + \rho_L(\mathbf{u}_L \cdot \nabla)\mathbf{u}_L = \nabla \cdot [-p_L \mathbf{I} + \eta_L(\nabla \mathbf{u}_L + (\nabla \mathbf{u}_L)^T)] + \rho_L \mathbf{g}$$

Vapor phase described using Weak form of Navier Stokes Equation :

$$\rho_v \frac{\partial \mathbf{u}_v}{\partial t} + \rho_v(\mathbf{u}_v \cdot \nabla)\mathbf{u}_v$$

$$= \nabla \cdot \left[-p_v \mathbf{I} + \eta_v(\nabla \mathbf{u}_v + (\nabla \mathbf{u}_v)^T) - \left(\frac{2}{3}\eta - \kappa_{dv}\right)(\nabla \cdot \mathbf{u})\mathbf{I}\right] + \rho_v \mathbf{g}$$

$$\frac{\partial \rho_v}{\partial t} + \nabla \cdot (\rho_v \mathbf{u}_v) = 0$$

Conduction Equation for the vapor phase:

$$\rho_v C_p \frac{\partial T_v}{\partial t} + \rho_v C_p(\mathbf{u}_v \cdot \nabla)T_v = -\nabla \cdot \kappa_v \nabla T_v$$

- State-of-the-Art Code developed in House.
- Study phase change risks in sCO2 compressors.
- Nucleation vs Residence time scales.
- Design effective sCO2 heat exchangers.
- Condensation and erosion predictions.

Boundary conditions at liquid-vapor phase boundary:

- 3 forces act on the liquid @ interface → natural boundary condition for liquid can be written as :

$$\mathbf{n} \cdot [-p_L \mathbf{I} + \eta_L(\nabla \mathbf{u}_L + (\nabla \mathbf{u}_L)^T)] = \dot{m}(\mathbf{u}_L - \mathbf{u}_v) + \sigma\kappa\mathbf{n} + \mathbf{n} \cdot [-p_v \mathbf{I} + \eta_v(\nabla \mathbf{u}_v + (\nabla \mathbf{u}_v)^T)]$$

reaction force due to the acceleration of the vapor away from the liquid surface

Surface Tension

Sum of pressure & viscous forces acting on the liquid from vapor

Phase Change and 2-PhaseFlow Model using Level Set Method

Water Boiling

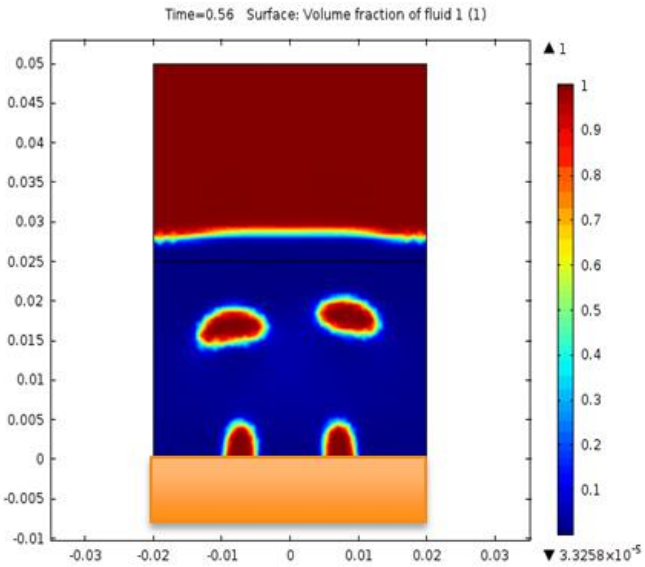

CO2 Boiling

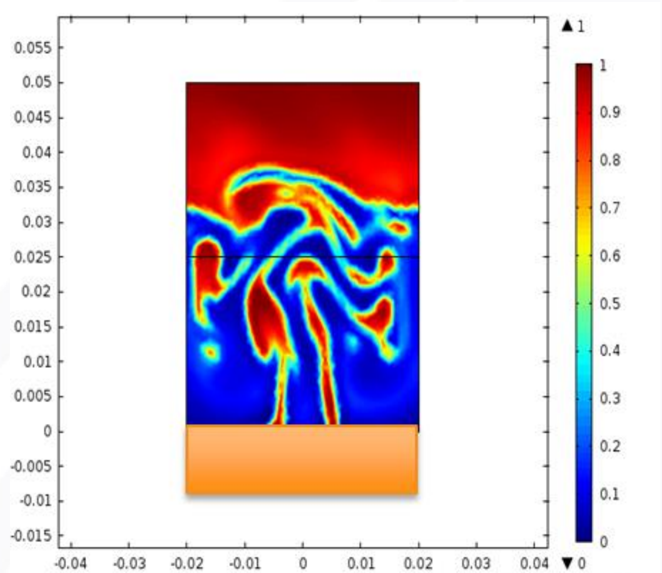

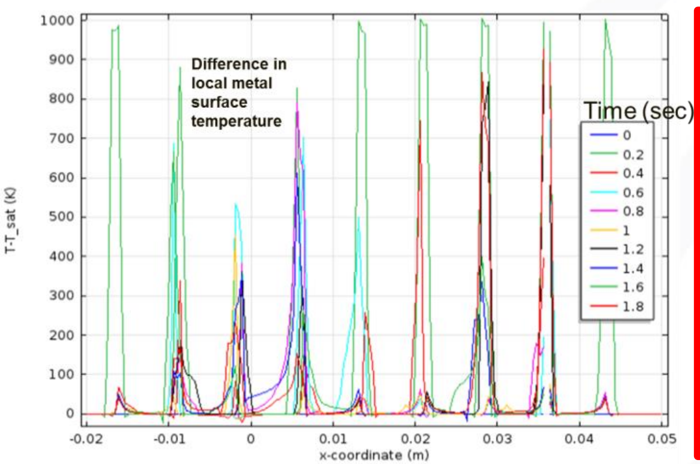

- Large local metal surface temp. rise.
- Uncertainty in HTCs
- Performance risks.
- Oxidation acceleration
- Life debit.

Transition to film boiling

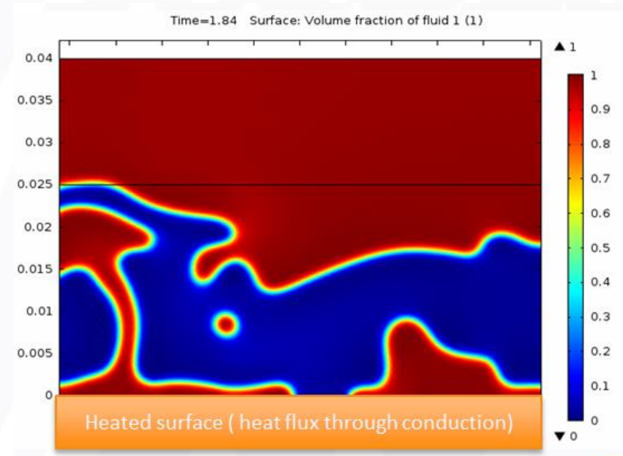

Phase Change and 2-PhaseFlow Model using Level Set Method

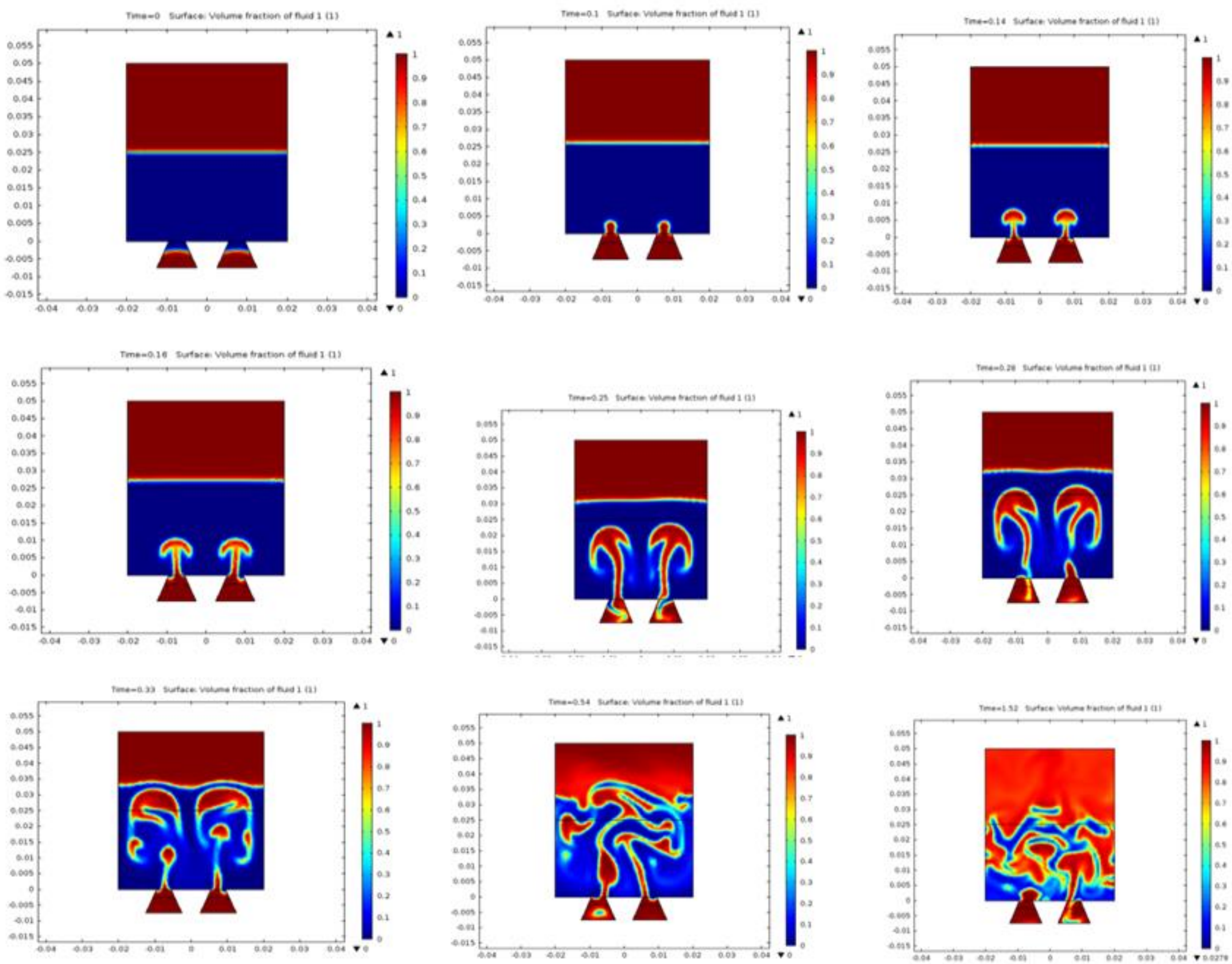

Dry Gas Seal Model Validation Tests in 10 MWe Sunshot sCO2 Expander

DGS panel + heating

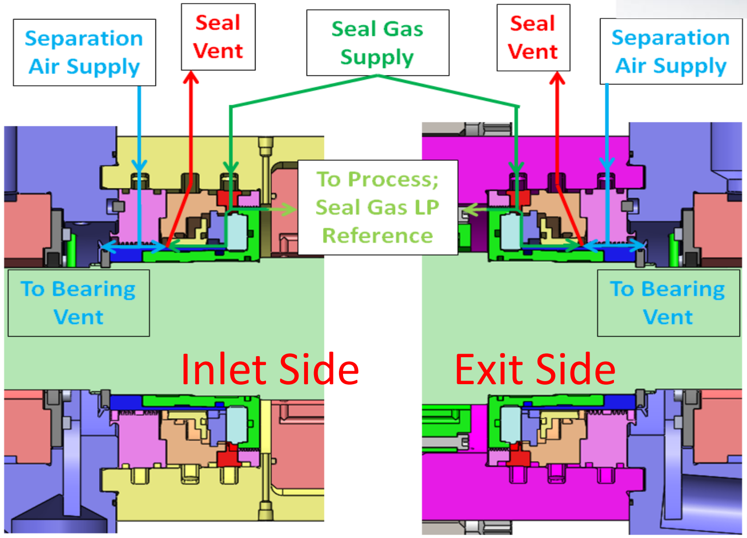

Stream	T (°C)	P (bara)
Seal Supply (CO_2)	100	89.6
Separation Air	26	1.19
Seal Vent		1.0

More details of DGS Model and Testing in : Thatte et.al , ASME Turbo Expo 2016, GT2016-57670

Low Cycle Fatigue Tests on Ni Alloys in sCO2

Low Cycle Fatigue Tests on Ni Alloys in sCO2

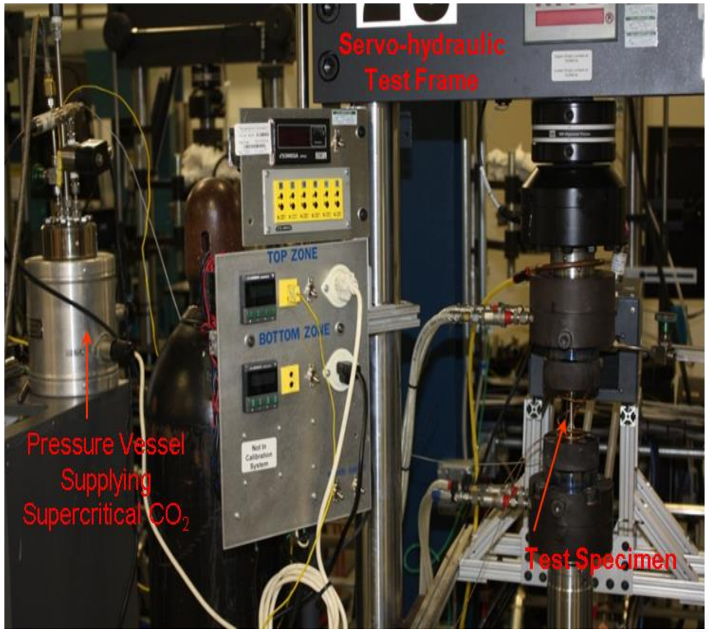

Inconel 617

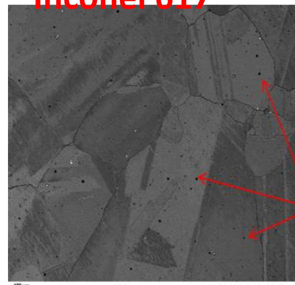

Intergranular particles (delta)

Transgranular particles (carbides)

Inconel 718

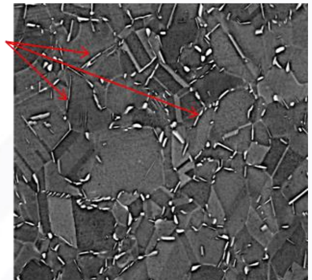

➢ **High corrosion resistance**
- Coarse grain
- Single phase alloy
- Cr rich

➢ **Good LCF properties**
- Fine grain
- Dual phase alloy
- Precipitates at grain boundaries

Find This

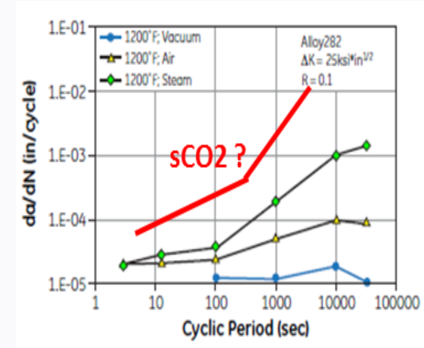

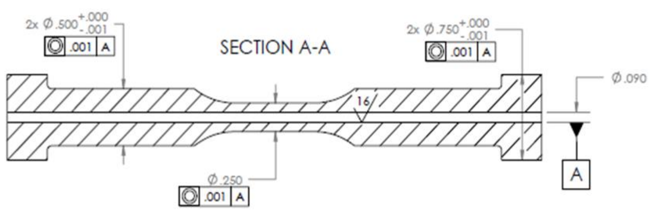

Thumbnail pattern of Natural crack initiation on sCO2 side

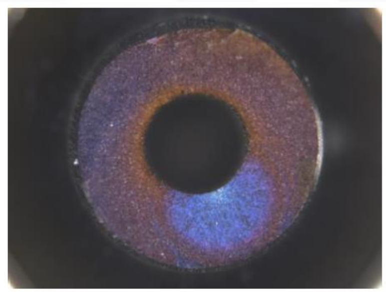

SEM of crack Initiation site

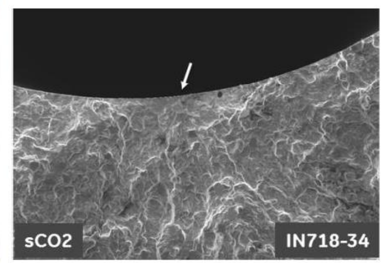

facetted grain showing slip plane cracking within the grain

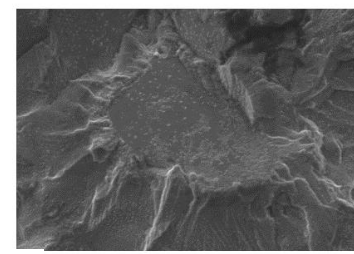

Tested in Air

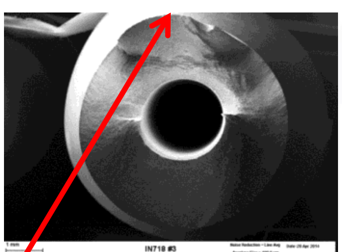

Failure initiated on the OD

Tested in sCO_2

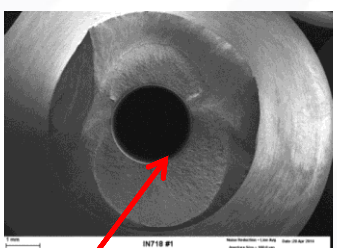

Failure initiated on the ID

16

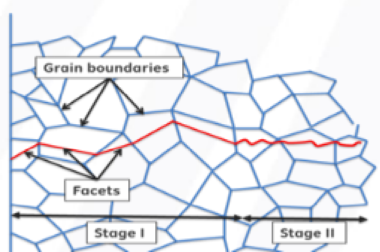

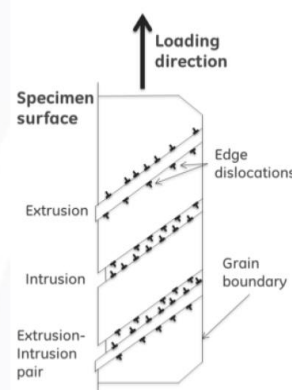

-Dislocation motion in most favorably orientated grains.
-Formation of extrusion and intrusion types of defects by dislocation accumulation

Differences in Air vs sCO2 Crack Initiation Mechanisms

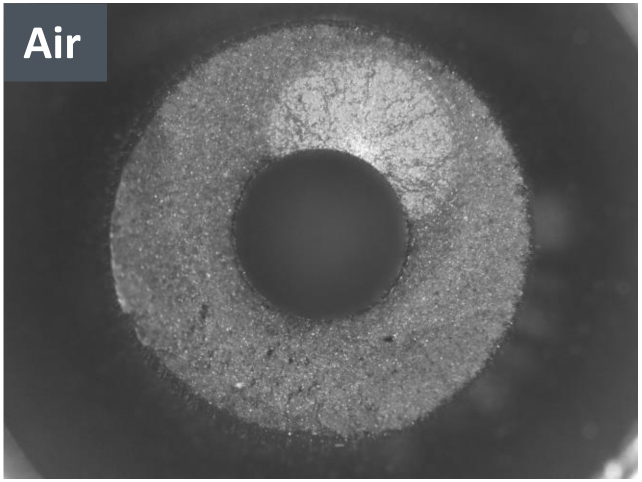

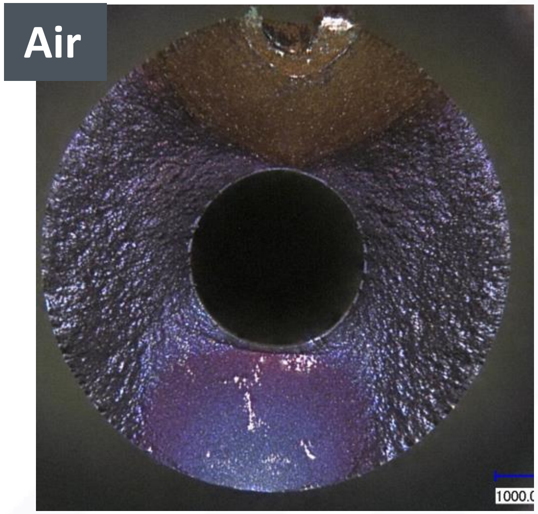

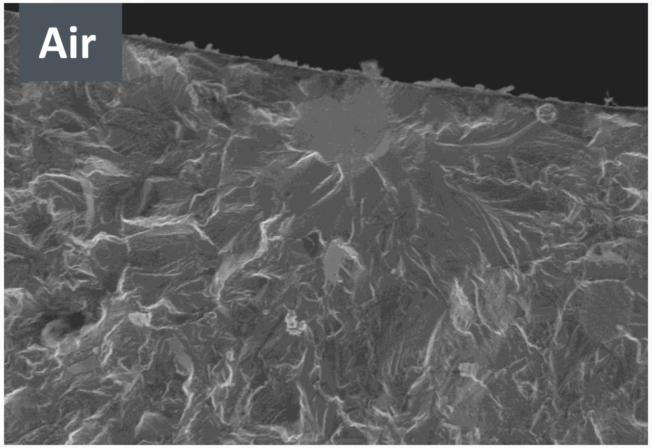

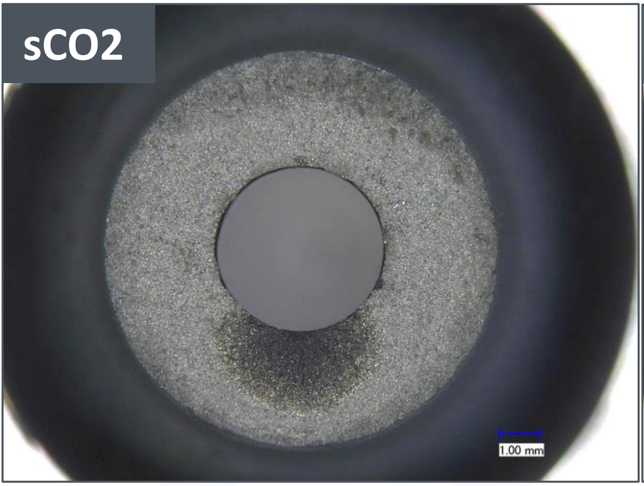

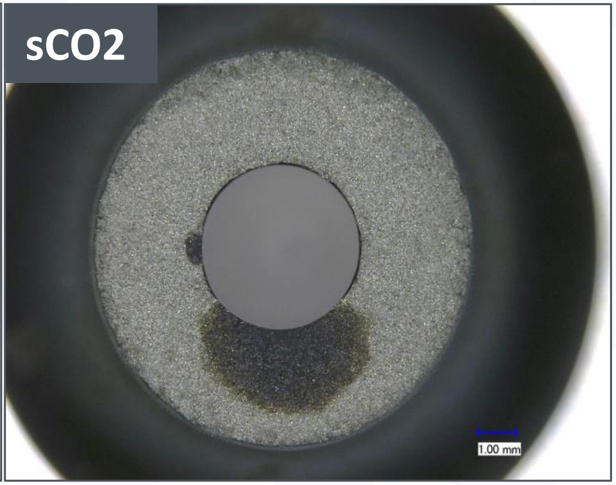

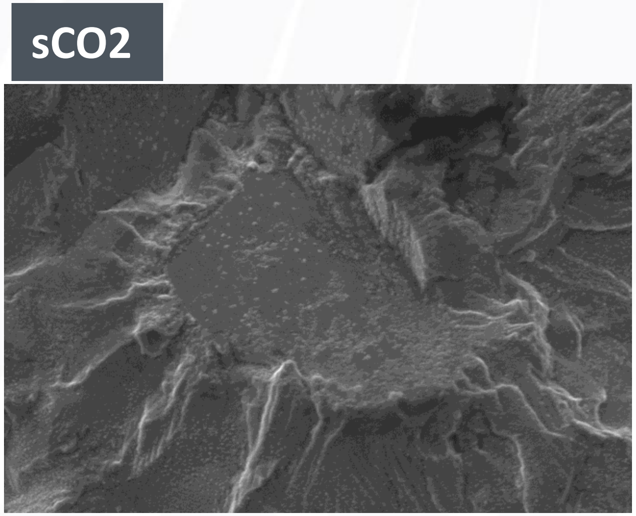

Low Cycle Fatigue Tests on Ni Alloys in sCO2

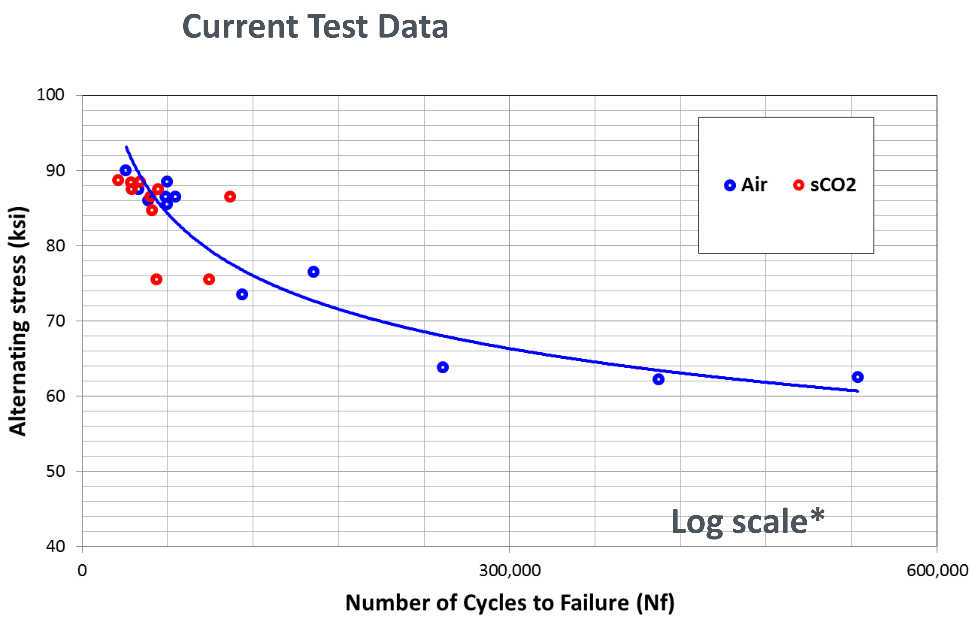

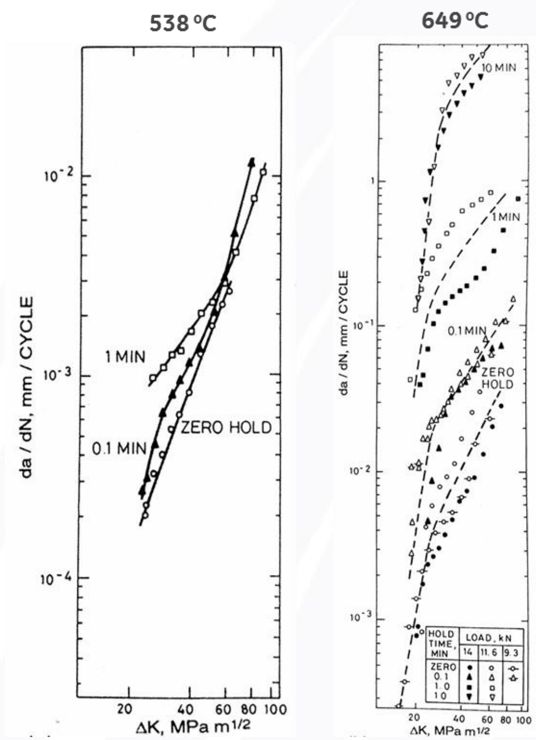

* Prior literature in air

- No significant LCF life debit is observed in IN718 by sCO_2 at 550°C, 0.7% max strain, 20 cpm.
- Little lower life observed for 0.5 % strains due to longer exposure times resulting from larger number of cycles to failure.
- It is expected that with longer hold-times, sCO2 environment may be more aggressive – resulting in lower fatigue life.

Corrosion of Ni base Super Alloys in sCO2

Corrosion of Ni base Super Alloys in sCO2

Find Species Diffusion using Spectroscopy

After: Layered structure from sCO2 corrosion

Before

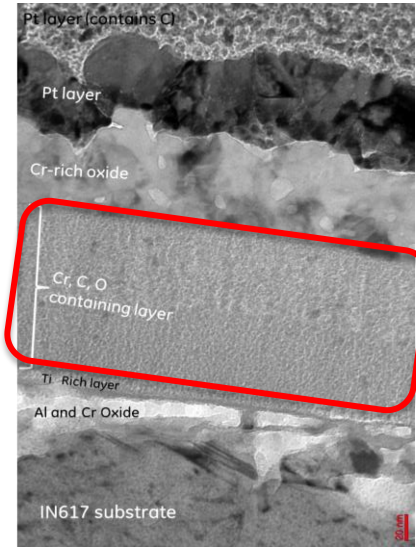

Elemental distribution map (EDS map) of IN617 area shown in (BF)

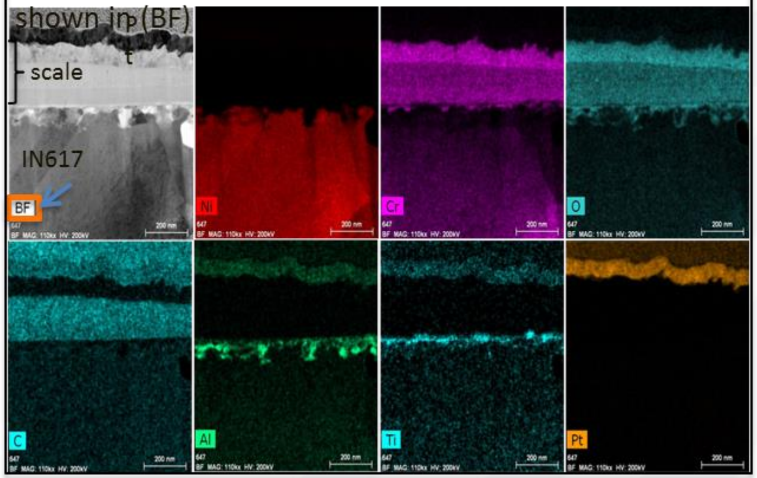

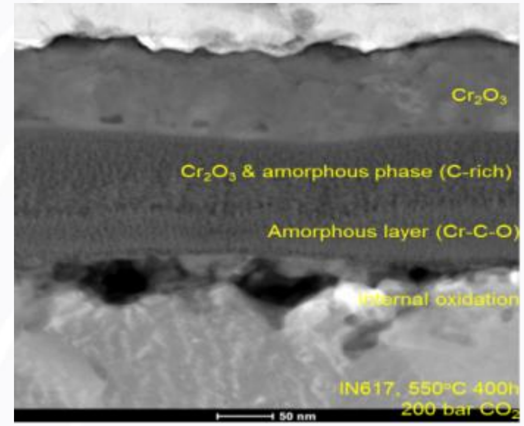

3 Types of sCO2 Corrosion Attacks

pitting **Internal attack** **Voids**

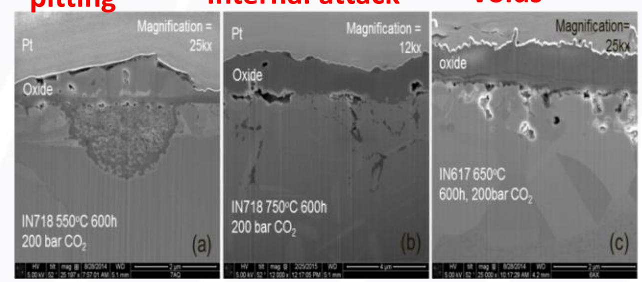

Evolution of Corrosion with Time & Temperature

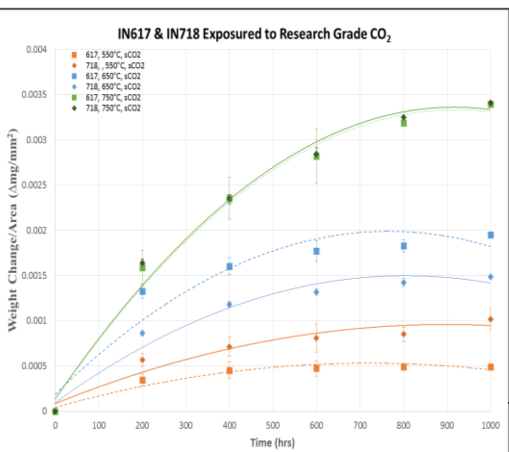

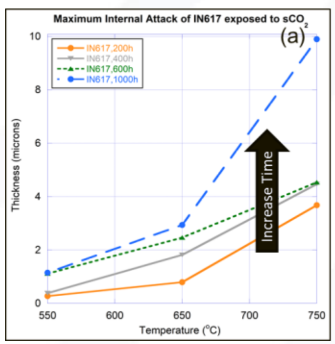

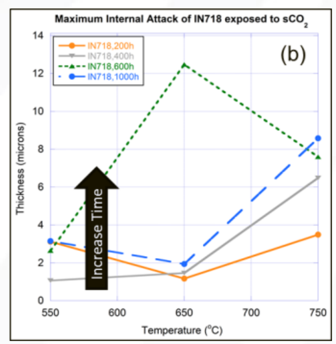

Chemical Kinetics Model

Alloys	Activation energy, Ea (Joules)
IN617	1.7×10^{5}
IN718	9.3×10^{4}

Effect on Surface Properties

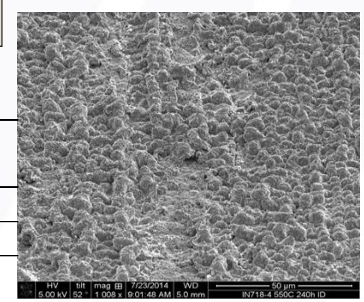

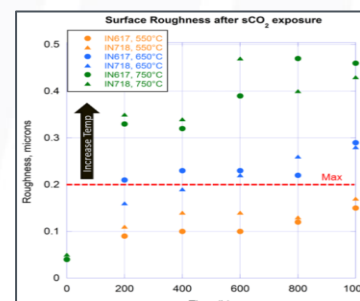

More details of sCO2 Corrosion in: Dheeradhada V., Thatte A., EPRI International Conference on Corrosion in Power Plants, 2015

Models for Crack Initiation, Crack Propagation & High Energy X-Ray Tomography

Models for Crack Initiation, Crack Propagation & High Energy X-Ray Tomography

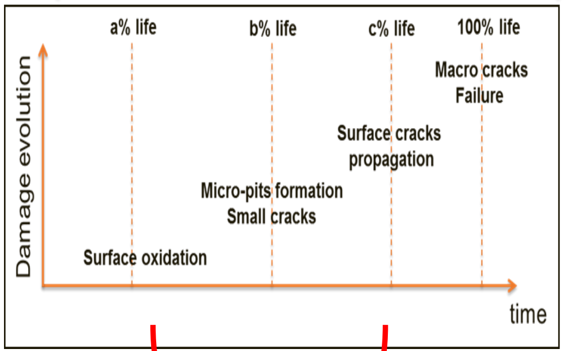

Chemistry & Thermodynamics coupled Crack Initiation Model:

$$N_i = A(\Delta\varepsilon_p)^{-m} exp\left(\frac{Q}{RT}\right)\left(\frac{1}{\nu} + t_h\right)^{-n}$$

Crack Initiation Model

6 GeV Synchrotron

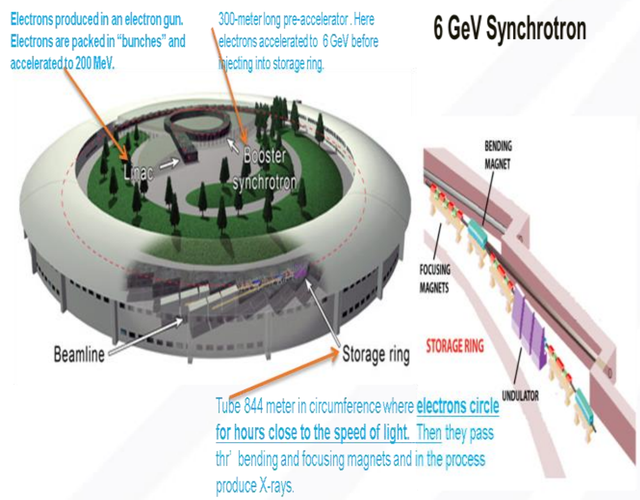

+

3D Crack Propagation Model

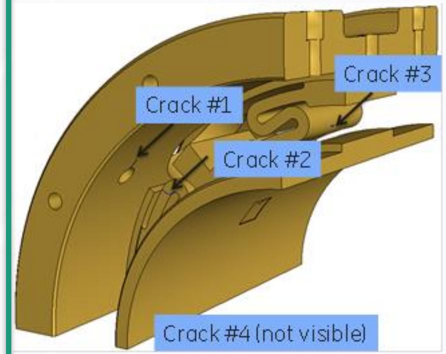

Predicts Crack Evolution in 3D and # of cycles to final failure

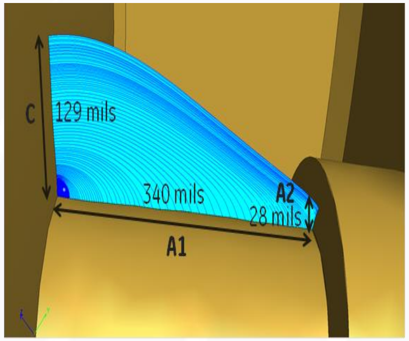

Predicted Crack Propagation Rate

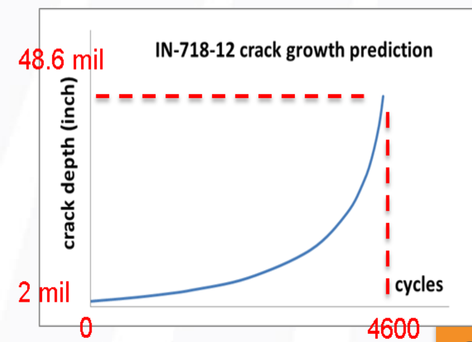

X-Ray Tomography

After 15000 cycles: No micro cracks

After 30000 cycles: 3D crack evolution captured Non-destructively

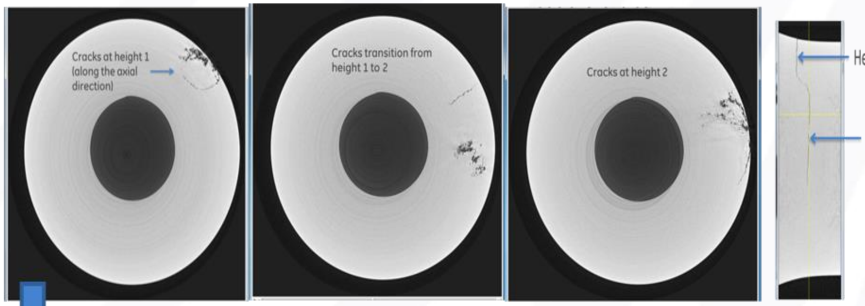

Digital Reconstruction of time evolution of 3D crack morphology

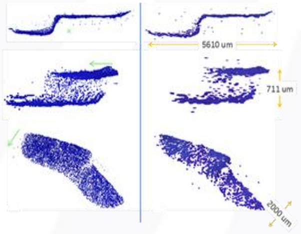

Using Bayesian Probabilistics Framework to Tie it All Together

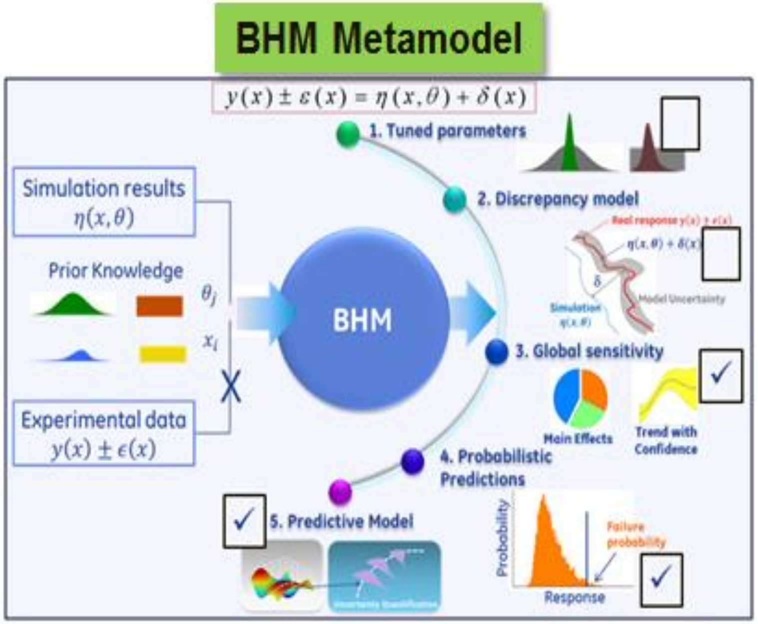

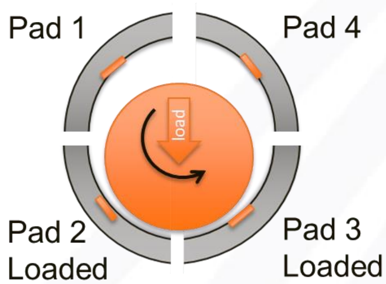

Principal Component Extraction

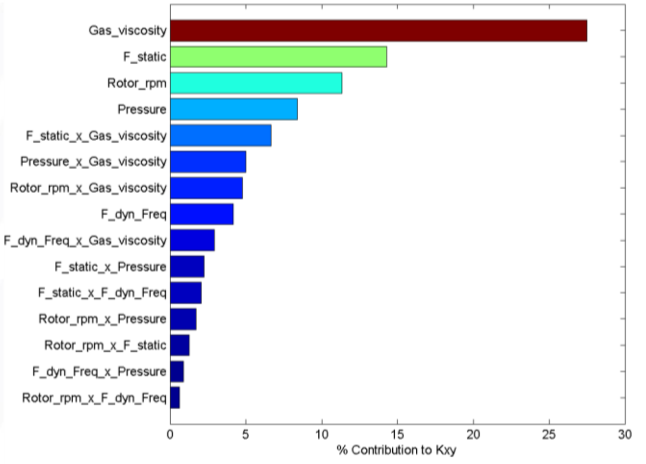

Uncertainty Prediction

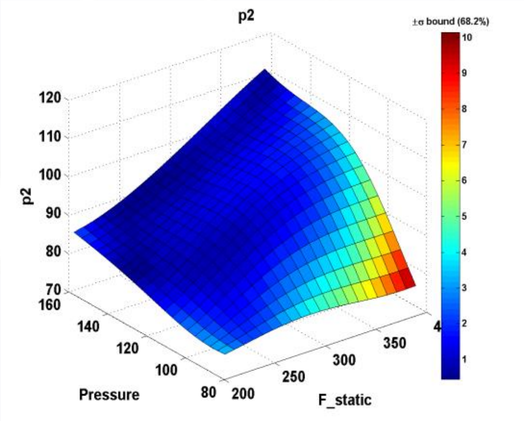

Statistically Relevant Life Prediction

Initiation Life (Arrhenius model)
+
Propagation Life (3DFAS)
=
Total Life

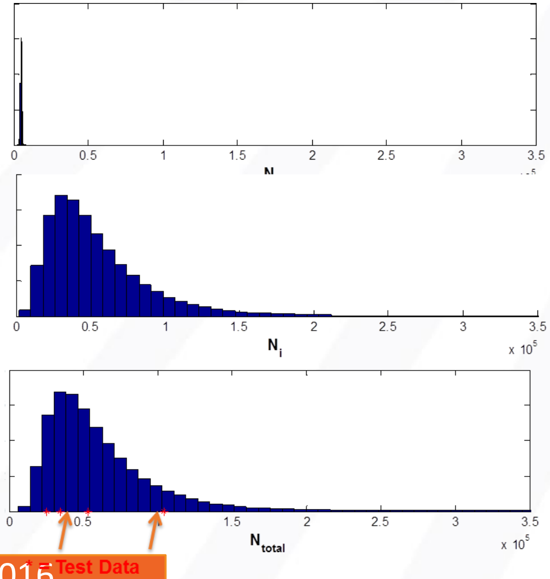

Model Predictions:

	Mean	Std
Ni	55,590	37,129
Np	5033	493.3
Ntotal	60,622	37,132

Milestones

Phase 1 (completed) :

- Performance models for DGS & HGB
- Sonic Transition Models
- sCO_2 Phase Change Models & Tests

Phase 2 (completed) :

- sCO_2 LCF and Corrosion Experiments
- sCO_2 Chemical Kinetics & Oxidation
- 3D Crack Propagation Models
- High Energy X-ray Tomography.

Phase 3 (in progress):

- Crack propagation tests in sCO_2
- Integrated Life Prediction Model
- Bayesian Probabilistics Performance and Life Framework

Path to Market

- Mature 10 MWe sCO2 turbine technology for CSP by 2020.
- DOE STEP Program: 50 MW Power Plant Demo
- 500 MW sCO2 turbine ~ 2025-2030
- Other Applications : Waste Heat Recovery , Transportation

Conclusions

- Multi-scale coupled physics models to predict dynamic performance of HGB and DGS are developed.
- The models try to capture sCO2 specific phenomena like sonic transitions, possibility of phase change, flow induced and rotordynamic instabilities and large perturbations in apparent heat transfer coefficients.
- The output of performance model is fed into 3D fracture mechanics based life prediction framework.
- Test campaigns to characterize corrosion of Nickel base super alloys in sCO2 environment are conducted and chemical kinetics models are built.
- LCF behavior of Ni base super alloys in high pressure, high temperature sCO2 is also being investigated using a novel experimental setup.
- Bayesian hybrid probabilistic models are developed to quantify uncertainty in multi-physics models and to validate models with statistical confidence.
- This coupled physics framework is a valuable tool to design a wide variety of sCO2 turbomachines and heat exchangers, analyze their performance in supercritical and trans-critical mission cycles and predict their life for long term durability of sCO2 turbomachines.